Inorganic Chemistry

Article

pubs.acs.org/IC

Derivation of Structure–Activity Relationships from the Anticancer Properties of Ruthenium(II) Arene Complexes with 2-Aryldiazole Ligands

Marta Martínez-Alonso,[†] Natalia Busto,[†] Félix A. Jalón,[‡] Blanca R. Manzano,[‡] José M. Leal,[†] Ana M. Rodríguez,[‡] Begoña García,*[,†] and Gustavo Espino*[,†]

[†]Departamento de Química, Facultad de Ciencias, Universidad de Burgos, Plaza Misael Bañuelos s/n, 09001 Burgos, Spain

[‡]Departamento de Química Inorgánica, Orgánica y Bioquímica, Facultad de Químicas (IRICA), Universidad de Castilla—La Mancha, Avenida Camilo J. Cela 10, 13071 Ciudad Real, Spain

Supporting Information

ABSTRACT: The ligands 2-pyridin-2-yl-1*H*-benzimidazole (HL^1), 1-methyl-2-pyridin-2-ylbenzimidazole (HL^2), and 2-(1*H*-imidazol-2-yl)pyridine (HL^3) and the proligand 2-phenyl-1*H*-benzimidazole (HL^4) have been used to prepare five different types of new ruthenium(II) arene compounds: (i) monocationic complexes with the general formula $[(\eta^6\text{-arene})RuCl(\kappa^2\text{-}N,N\text{-}HL)]Y$ [HL = HL^1, HL^2, or HL^3; Y = Cl or BF_4; arene = 2-phenoxyethanol (phoxet), benzene (bz), or *p*-cymene (*p*-cym)]; (ii) dicationic aqua complexes of the formula $[(\eta^6\text{-arene})Ru(OH_2)(\kappa^2\text{-}N,N\text{-}HL^1)](Y)_2$ (Y = Cl or TfO; arene = phoxet, bz, or *p*-cym); (iii) the nucleobase derivative $[(\eta^6\text{-arene})Ru(9\text{-MeG})(\kappa^2\text{-}N,N\text{-}HL^1)](PF_6)_2$ (9-MeG = 9-methylguanine); (iv) neutral complexes consistent with the formulation $[(\eta^6\text{-arene})RuCl(\kappa^2\text{-}N,N\text{-}L^1)]$ (arene = bz or *p*-cym); (v) the neutral cyclometalated complex $[(\eta^6\text{-}p\text{-cym})RuCl(\kappa^2\text{-}N,C\text{-}L^4)]$. The cytototoxic activity of the new ruthenium(II) arene compounds has been evaluated in several cell lines (MCR-5, MCF-7, A2780, and A2780cis) in order to establish structure–activity relationships. Three of the compounds with the general formula $[(\eta^6\text{-arene})RuCl(\kappa^2\text{-}N,N\text{-}HL^1)]Cl$ differing in the arene moiety have been studied in depth in terms of thermodynamic dissociation constants, aquation kinetic constants, and DNA binding measurements. The biologically most active compound is the *p*-cym derivative, which strongly destabilizes the DNA double helix, whereas those with bz and phoxet have only a small effect on the stability of the DNA double helix. Moreover, the inhibitory activity of several compounds toward CDK1 has also been evaluated. The DNA binding ability of some of the studied compounds and their CDK1 inhibitory effect suggest a multitarget mechanism for their biological activity.

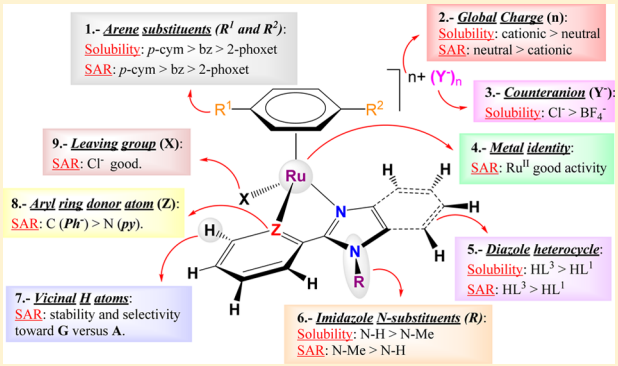

INTRODUCTION

Cancer embraces a broad collection of heinous diseases, characterized by the uncontrolled proliferation of abnormal cells that invade and disrupt tissues. It begins at specific organs and often spreads to more distant parts of the body through the lymphatic system or bloodstream to extend their destructive growth.[1] The causes responsible for the initiation and promotion of cancer may be both external (e.g., chemicals, radiation, viruses) and internal (e.g., hormones, immune conditions, inherited genes).[2] The treatment of cancer is accomplished by a number of optional therapies such as surgery, chemotherapy, radiation therapy, immunotherapy, and monoclonal antibody therapy. In particular, chemotherapy involves the use of drugs to kill cancer cells by interfering with cell division processes in different possible ways, e.g., with the duplication of DNA. Therefore, anticancer drugs tend to target all rapidly dividing cells, generally with low specificity for cancer cells.[3]

Recently, half-sandwich ruthenium(II) arene compounds[4] have been identified as an alternative class of potential anticancer drugs that could complement the medicines nowadays in clinical use, such as cisplatin and congeners.[5] In particular, several compounds of the general formulas $[(\eta^6\text{-arene})RuX(\kappa^2\text{-}N,N\text{-}L)]Y$ have displayed promising anticancer activity. The previous compounds are typically endowed with four structural elements in the coordination sphere of the Ru^{II} center: (i) an η^6-arene moiety, which stabilizes the oxidation state of the metal cation and may facilitate transport through the cell membrane, (ii) a leaving group (X), which undergoes easy dissociation to allow coordination of the metal ion to target biomolecules, (iii) an ancillary bidentate ligand (κ^2-*N*,*N*-L), which may control the reactivity toward different biomolecules (DNA, enzymes) and even play a key role in

Received: August 6, 2014

   dx.doi.org/10.1021/ic501865h | *Inorg. Chem.* XXXX, XXX, XXX–XXX

Scheme 1. Structure and Numbering of the New Ruthenium(II) Arene Compounds with Aryl-Substituted Benzoazoles

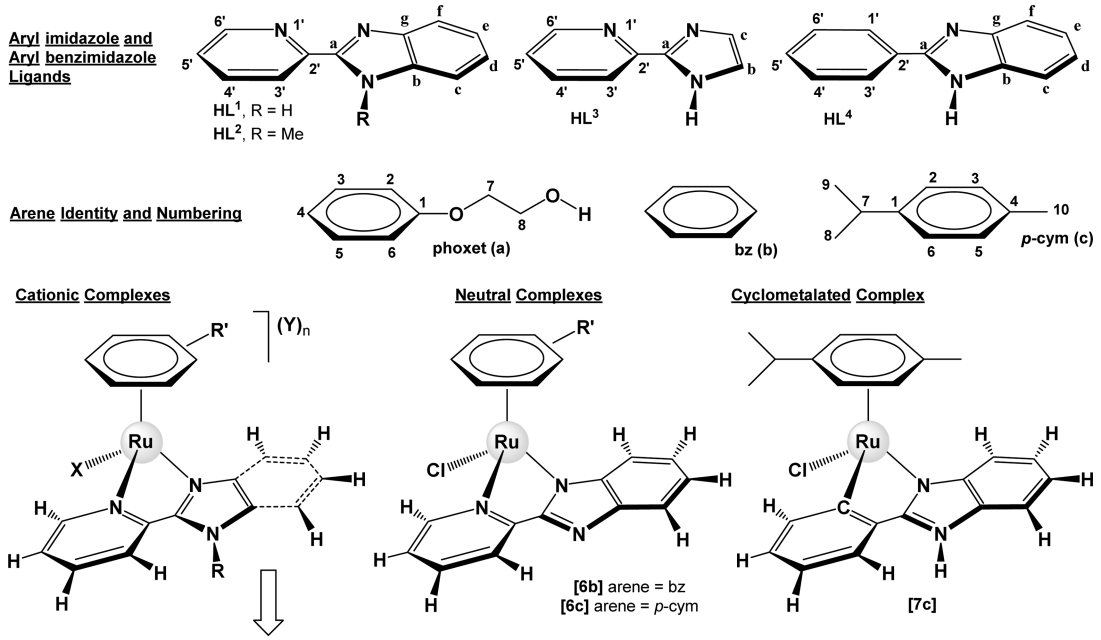

Labeling of Cationic Compounds

[Cation]Y_n	[1a]Cl [1a](BF_4)	[1b]Cl [1b](BF_4)	[1c]Cl [1c](BF_4)	[2c]Cl	[3c]Cl	[4a]$(BF_4)_2$ [4a]$(TfO)_2$	[4b]$(BF_4)_2$ [4b]$(TfO)_2$	[4c]$(BF_4)_2$ [4c]$(TfO)_2$	[5c]$(PF_6)_2$
Ligand	HL^1	HL^1	HL^1	HL^2	HL^3	HL^1	HL^1	HL^1	HL^1
Arene	phoxet	bz	*p*-cym	*p*-cym	*p*-cym	phoxet	bz	*p*-cym	*p*-cym
X	Cl	Cl	Cl	Cl	Cl	H_2O	H_2O	H_2O	9-MeG

the interaction with them through hydrogen bonding or intercalation, and (iv) the overall charge and counterion identity, which can affect the solubility and permeability.[6] Our group has reported recently the synthesis and anticancer properties of other families of ruthenium(II) arene complexes with ligands such as 2,4-diamino-6-(2-pyridyl)-1,3,5-triazine (2-pydaT),[7] several phenanthrolines,[8] or the aminophosphines 2-(diphenylphosphino)-1-methylimidazole (dpim) and diphenyl-2-pyridylphosphine (Ph_2Ppy).[9] This work is focused on the combination of different ruthenium(II) arene fragments with aryl-substituted benzimidazoles as bioactive ancillary ligands, in the hope that the resulting ruthenium(II) complexes can improve the antiproliferative properties of the free ligands.

Benzimidazoles and, in particular, aryl-substituted benzimidazole derivatives exhibit a wide slate of potential pharmaceutical applications, including antihypertensive, antiinflammatory, antibacterial, antifungal, antiviral, antioxidant, antiulcer, and antitumor activity.[10,11] Furthermore, some examples of palladium(II) and platinum(II) complexes with 2-(2-pyridyl)-benzimidazole have been studied in relation to their cytotoxicity.[12] What is more, novel families of ruthenium(II) complexes bearing benzimidazole scaffolds in the ancillary ligands have been reported over the last months as potential anticancer[6b−d] and antidiabetes[13] drugs. In this contribution, we describe the preparation and characterization of several ruthenium(II) complexes with the ligands 2-pyridin-2-yl-1*H*-benzimidazole (HL^1), 1-methyl-2-pyridin-2-ylbenzimidazole (HL^2), and 2-(1*H*-imidazol-2-yl)pyridine (HL^3) and deprotonated 2-phenyl-1*H*-benzimidazole (HL^4) (see Scheme 1), as well as their cytotoxic activity against several cancer cell lines, to establish the corresponding structure−activity relationships (SAR) and thus the effect of different chemical functions in structural elements such as the arene, the counterion, the leaving group, the specific ancillary ligand (aryl-substituted benzimidazoles), and the overall charge of the complexes. In earlier contributions, we verified that ruthenium coordinates to the N7 guanine site, whereas aromatic ligands can either intercalate or not, depending on their structure. Bifunctional complexes have aroused great interest because of the observation that these types of compounds with dual action (intercalation into the base pairs and metal coordination to the DNA bases)[14,15] promote unusual distortion of DNA that affects the recognition of repair enzymes, leading to apoptosis and cell death. Ruthenium arene complexes endowed with such ability display much higher cytotoxicity toward cancer cells than the corresponding nonintercalant compounds. Nevertheless, it should be noticed that other biotargets such as kinase proteins or topoisomerases can also be related to the biological activity of these complexes.[16,17]

RESULTS AND DISCUSSION

Synthesis and Structural Characterization of Compounds. The synthesis and characterization of all of the new compounds are described in detail in the Supporting Information (SI).

a. Cationic Complexes. The reaction between the appropriate ruthenium(II) arene starting material and the ligands HL^1, HL^2, and HL^3 (molar ratio 1:2) at room

dx.doi.org/10.1021/ic501865h | *Inorg. Chem.* XXXX, XXX, XXX−XXX

Scheme 2. Synthesis of the New Ruthenium(II) Compounds

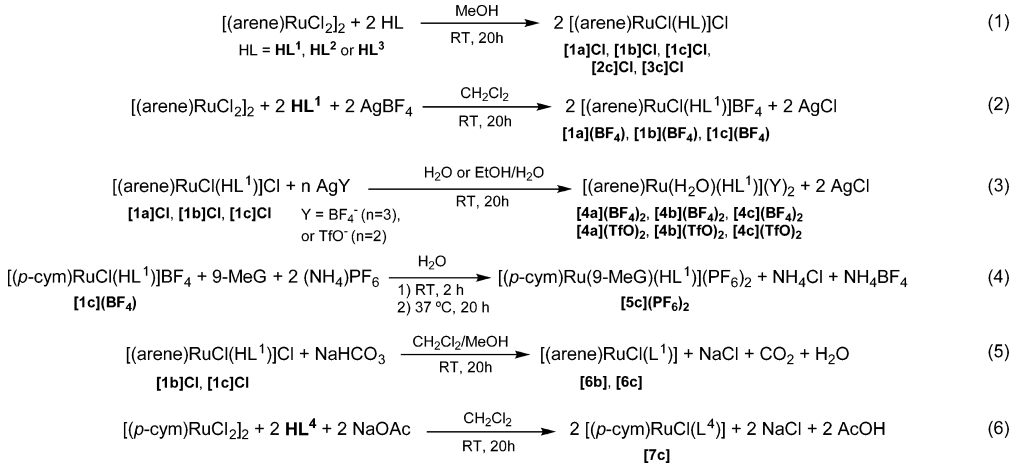

temperature and using methanol as the solvent yielded compounds of the general formula $[(\eta^6\text{-arene})RuCl(\kappa^2\text{-}N,N\text{-}HL)]Cl$ [HL = HL^1, arene = 2-phenoxyethanol (phoxet; **[1a]Cl**), benzene (bz; **[1b]Cl**), or *p*-cymene (*p*-cym; **[1c]Cl**); HL = HL^2, arene = *p*-cym (**[2c]Cl**); HL = HL^3, arene = *p*-cym (**[3c]Cl**); see Scheme 1 and eq 1 in Scheme 2]. The respective BF_4^- salts of the general formula $[(\eta^6\text{-arene})RuCl(\kappa^2\text{-}N,N\text{-}HL^1)]BF_4$ [arene = phoxet (**[1a](BF$_4$)**), bz (**[1b](BF$_4$)**), or *p*-cym (**[1c](BF$_4$)**)] were prepared by a related procedure in the presence of $AgBF_4$ and using CH_2Cl_2 as the solvent (see Scheme 1 and eq 2 in Scheme 2).

The dicationic aqua derivatives of the formula $[(\eta^6\text{-arene})Ru(OH_2)(\kappa^2\text{-}N,N\text{-}HL^1)](Y)_2$ [arene = phoxet (**[4a](BF$_4$)$_2$** and **[4a](TfO)$_2$**), bz (**[4b](BF$_4$)$_2$** and **[4b](TfO)$_2$**), *p*-cym (**[4c](BF$_4$)$_2$** and **[4c](TfO)$_2$**); see Scheme 1] were also synthesized and isolated by treating the compounds **[1a]Cl**, **[1b]Cl**, and **[1c]Cl** with either an excess of $AgBF_4$ (molar ratio 1:3) or AgTfO (molar ratio 1:2) in distilled water (see eq 3 in Scheme 2). The nucleobase derivative $[(\eta^6\text{-arene})Ru(9\text{-MeG})(\kappa^2\text{-}N,N\text{-}HL^1)](PF_6)_2$ [**[5c](PF$_6$)$_2$**; see Scheme 1] was prepared by reacting **[1c](BF$_4$)** with 9-methylguanine (9-MeG) at 37 °C in water and isolated as the PF_6^- salt by adding an excess of $(NH_4)PF_6$ (see eq 4 in Scheme 2).

b. Neutral Complexes. In addition, the compounds **[1b]Cl** and **[1c]Cl** were reacted with $NaHCO_3$ in a mixture of dichloromethane/methanol at room temperature to produce the neutral complexes $[(\eta^6\text{-arene})RuCl(\kappa^2\text{-}N,N\text{-}L^1)]$ [L^1 = deprotonated HL^1; arene = bz (**[6b]**) or *p*-cym (**[6c]**); see Scheme 1 and eq 5 in Scheme 2].[18]

c. Cyclometalated Complex. On the other hand, the addition of the commercial proligand HL^4 to a solution of $[(\eta^6\text{-}p\text{-cym})RuCl_2]_2$ in dichloromethane in the presence of NaAcO (molar ratio 2:1:2) at room temperature resulted in the formation of the cyclometalated complex $[(\eta^6\text{-}p\text{-cym})RuCl(\kappa^2\text{-}N,C\text{-}L^4)]$ (**[7c]**; see Scheme 1 and eq 6 in Scheme 2).[19]

All of the new compounds were isolated in moderate-to-good yield (from 43% to 85%) as the corresponding racemates (R_{Ru} or S_{Ru}) in the form of yellow, orange, or brown solids that are air- and moisture-stable. Qualitative tests have determined that the salts of monocationic and dicationic complexes of types $[(\eta^6\text{-arene})RuCl(\kappa^2\text{-}N,N\text{-}HL^1)]Y$ and $[(\eta^6\text{-arene})Ru(OH_2)(\kappa^2\text{-}N,N\text{-}HL^1)](Y)_2$ are soluble in water and in most cases also in other polar solvents such as methanol and ethanol (see the Experimental Section). Neutral complexes **[6b]** and **[6c]** are also slightly soluble in water, but **[7c]** is only soluble in some organic solvents such as dichloromethane, chloroform, acetone, and dimethyl sulfoxide (see Table 2 for quantitative tests).

All of the aforementioned derivatives have been fully characterized by ^1H and $^{13}C\{^1H\}$ NMR spectroscopy and also by IR spectroscopy, positive fast-atom-bombardment (FAB^+) mass spectrometry, molar conductivity, and elemental analysis. In addition, the $^{19}F\{^1H\}$ NMR spectra have been recorded for the BF_4^-, PF_6^-, and TfO^- salts and the $^{31}P\{^1H\}$ NMR spectra for the PF_6^- salts. Assignment of all of the peaks in the ^1H and $^{13}C\{^1H\}$ NMR spectra of every complex was performed using 2D NMR experiments such as $^1H-^1H$ gCOSY, $^1H-^1H$ NOESY, $^1H-^{13}C$ gHSQC, and $^1H-^{13}C$ gHMBC (see the Experimental Section and Tables 1SI-a–c in the SI) and corroborated with bibliographic data of palladium or platinum complexes with HL^1, $[MCl_2(HL^1)]$ (M = Pd or Pt).[12a] The crystal structures of compounds **[1a]Cl**, **[1b](BF$_4$)**, **[1c](BF$_4$)**, **[2c]Cl**, $\{[\mathbf{4b}]_2(BF_4)_2(SiF_6)\}$, **[5c](PF$_6$)$_2$**, and **[7c]** have been determined by single-crystal X-ray diffraction.

The ^1H NMR spectra of the monocationic compounds **[1a]Cl**, **[1a](BF$_4$)**, **[1b]Cl**, **[1b](BF$_4$)**, **[1c]Cl**, **[1c](BF$_4$)**, **[2c]Cl**, and **[3c]Cl** in DMSO-d_6 or $CDCl_3$ at 25 °C proved coordination of the corresponding ligands to the respective metallic fragments. Explicitly, the characteristic signals for HL^1, HL^2, and HL^3 in the complexes are downfield-shifted in all cases with regard to those of the free ligands. Regardless of the ligand, $H^{6'}$(py) exhibits the strongest shift with a $\Delta\delta$ (^1H) = 0.68–0.99 ppm (see Figure 1SI-a in the SI). The complexes with HL^1 and HL^3 also display a broad resonance attributed to the N–H group, at about 15 and 16 ppm, respectively. Moreover, in the cases of the *p*-cym and phoxet derivatives, the NMR patterns of the arene resonances certify the asymmetric nature of the resulting complexes. Indeed, two doublets for diastereotopic methyls (^{i}Pr group) and the expected ABCD spin system for the aromatic resonances are observed in the *p*-cym derivatives, whereas in the case of the phoxet analogues, the two protons of the methylene groups are seen as diastereotopic and the aromatic protons produce an ABCDE pattern. The bz relatives, **[1b]Cl** and **[1b](BF$_4$)**, do not provide this kind of symmetry information; instead, they exhibit just the typical singlet at 6.30 ppm. Besides, the resonances for the aromatic protons (C–H) of the arenes in all of these complexes are upfield-shifted with regard to those of the free

dx.doi.org/10.1021/ic501865h | Inorg. Chem. XXXX, XXX, XXX–XXX

arene rings but downfield-shifted with respect to those of the dimeric precursors (see Tables 1SI-b and 1SI-c in the SI). On the other hand, the 2D ^{1}H−^{1}H NOESY spectrum for [**1c**](**BF$_4$**) (see Figure 2SI in the SI) shows nuclear Overhauser effect (NOE) cross peaks between the signal attributed to residual H_2O and those for $H^{3'}$ and H^c, suggesting that a H_2O molecule could be hydrogen-bonded to the N−H group of the coordinated HL^1 ligand (in fact, the crystal X-ray structure of [**1c**](**BF$_4$**) exhibits a H_2O molecule hydrogen-bonded to HL^1 in the solid state). What is more, this NOESY spectrum exhibits exchange peaks that correlate the broad resonances of H_2O and the −NH group, proving that these protons take part in an exchange process.

The ^{1}H NMR spectra of the aqua derivatives [**4a**](**BF$_4$**)$_2$, [**4b**](**BF$_4$**)$_2$, [**4c**](**BF$_4$**)$_2$, [**4a**](**TfO**)$_2$, [**4b**](**TfO**)$_2$, and [**4c**](**TfO**)$_2$ in D_2O at 25 °C are very similar to those of [**1a**]**Cl**, [**1b**]**Cl**, and [**1c**]**Cl**. However, most of the signals of the corresponding aromatic protons are shifted to higher frequencies relative to their chlorido precursors. This tendency has been previously observed for other dicationic aqua complexes.[7] Another interesting feature has been found in the 2D ^{1}H−^{1}H NOESY or 2D ^{1}H−^{1}H ROESY spectra of the aqua complexes [**4a**](**BF$_4$**)$_2$, [**4c**](**BF$_4$**)$_2$, [**4a**](**TfO**)$_2$, and [**4c**](**TfO**)$_2$. They exhibit exchange peaks between H^2 and H^6 and most likely also between H^3 and H^5, although the latter are completely or partially overlapped with diagonal cross-peaks (see Figure 1). This evidence suggests an interconversion

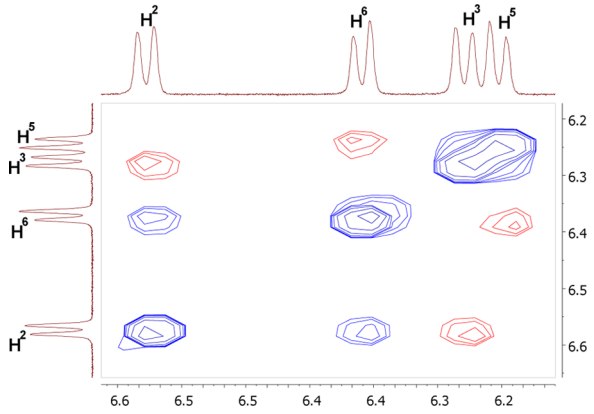

Figure 1. Zoom for the aromatic protons of *p*-cym in the 2D ^{1}H−^{1}H NOESY spectra of compound [**4c**](**BF$_4$**)$_2$ in D_2O at 25 °C. Red cross peaks = NOE correlations. Blue cross peaks out of the diagonal = exchange correlations.

process between the two possible enantiomers (R_{Ru} and S_{Ru}) of each complex.[20] Such a process seems to be slow in the NMR time scale at 25 °C because the signals involved in the exchange are clearly distinguishable. Bearing in mind that similar processes have not been witnessed for the corresponding chlorido precursors, we propose a mechanism that involves dissociation of the H_2O molecule and recoordination by the opposite site (Figure 2). This observation proves the higher lability of the aqua ligands in these complexes relative to chlorido ligands in the respective precursors. Significantly, fast inversion of the Ru center has been reported for chloridoruthenium(II) arene complexes with anionic O,O-donor ligands in protic solvents at room temperature, as established by the presence of only two doublets for the aromatic *p*-cym protons in chiral-at-metal complexes, suggesting a rapid exchange process between both enantiomers.[21]

The ^{1}H NMR spectrum of [**5c**](**PF$_6$**)$_2$) in DMSO-d_6 shows characteristic signals for coordinated 9-MeG and HL^1. A 2D ^{1}H−^{1}H ROESY experiment was recorded to assign all of the signals (see Figure 3SI in the SI). It is worth noting that nuclear Overhauser interactions were observed between the signals of residual H_2O and both $H^{3'}$ and H^c, suggesting that a H_2O molecule is hydrogen-bonded to the −NH group of the benzimidazole motif in solution (Scheme 3). What is more, an

Scheme 3. Structure, Numbering, and Significant NOE Contacts for [5c](PF$_6$)$_2$ with a Hydrogen-Bonded H_2O Molecule in the Second Coordination Sphere, as Observed by 2D ^{1}H−^{1}H ROESY in DMSO-d_6

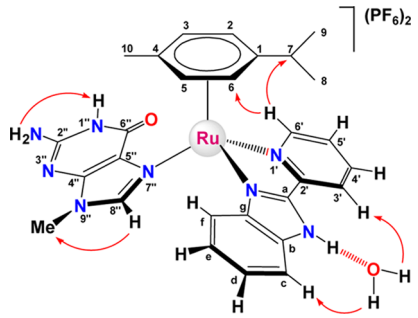

exchange cross-peak was detected between the N−H group and the H_2O molecule. Interestingly, the $H^{6'}$ resonance of [**5c**](**PF$_6$**)$_2$ is strongly shifted to higher frequencies (9.98 ppm) compared to the respective signal in [**1c**](**BF$_4$**) (9.62 ppm). This fact could be the result of both the dicationic nature of [**5c**]$^{2+}$ and the possible participation in solution of this proton in a hydrogen-bonding interaction with the O atom of 9-MeG, as is also pointed out by X-ray diffraction in the solid state (vide infra).

The ^{1}H NMR spectra of the neutral complexes [(η^6-arene)RuCl(κ^2-*N*,*N*-L^1)] [arene = bz ([**6b**]), *p*-cym ([**6c**])] in DMSO-d_6 show resonances for both the corresponding arene and deprotonated HL^1, labeled as L^1. Indeed, the absence of signals in the low-field region of both spectra confirmed

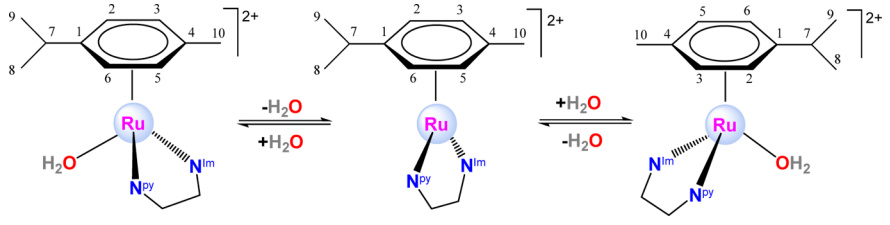

Figure 2. Proposed mechanism for the interconversion process between the two possible enantiomers (R_{Ru} and S_{Ru}) of the aqua complex [**4c**]$^{2+}$. A analogous mechanism is proposed for [**4a**]$^{2+}$.

dx.doi.org/10.1021/ic501865h | *Inorg. Chem.* XXXX, XXX, XXX−XXX

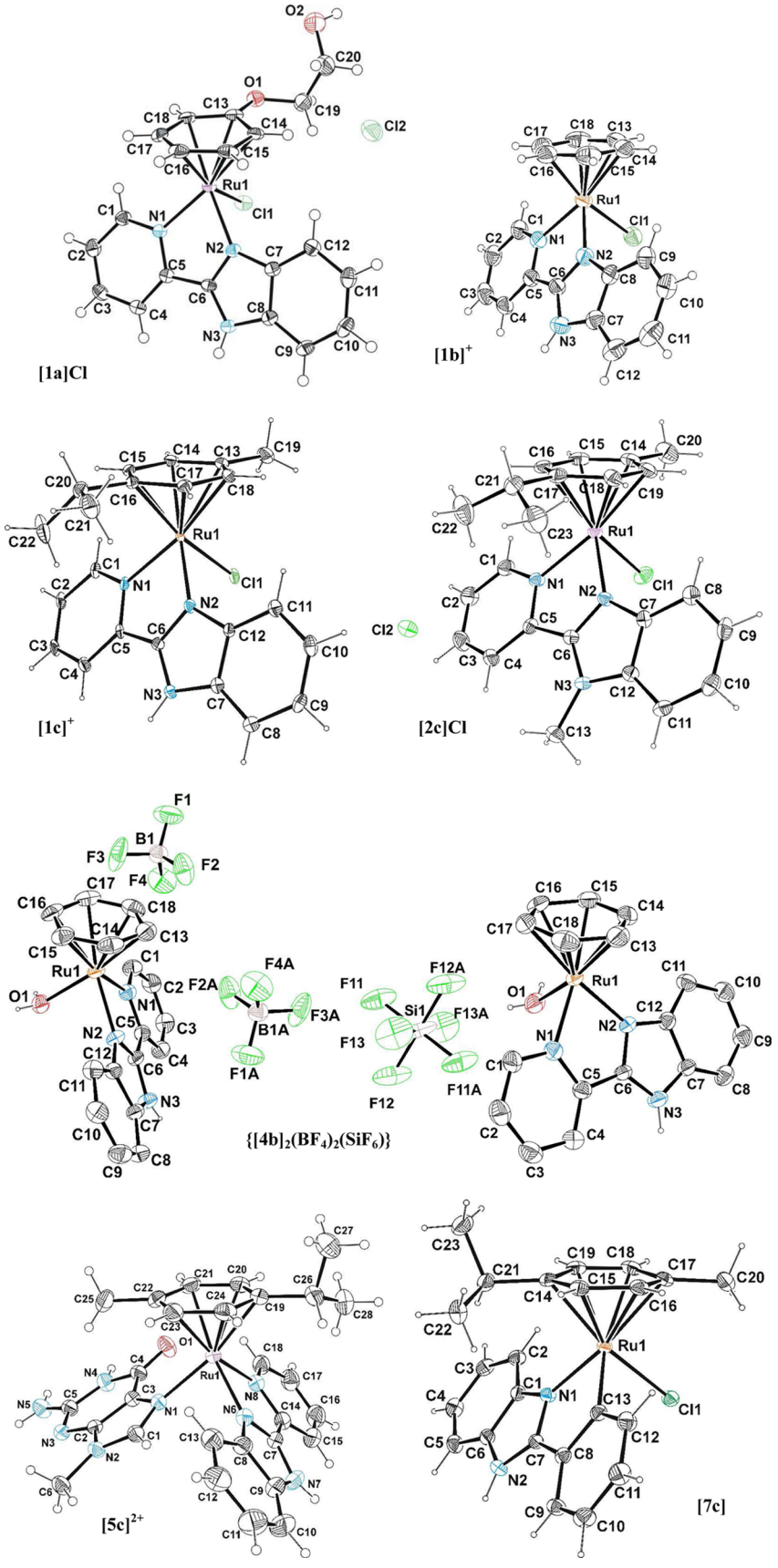

Figure 3. ORTEP diagrams for compounds [**1a**]**Cl**·2H_2O, [**1b**](BF_4)·2H_2O, [**1c**](BF_4)·H_2O, [**2c**]**Cl**, {[**4b**](BF_4)(SiF_6)$_{0.5}$}·2H_2O, [**5c**](PF_6)$_2$·H_2O, and [**7c**]. Water molecules and, in some cases, counteranions have been omitted for space reasons. Thermal ellipsoids are shown at the 30% probability.

dx.doi.org/10.1021/ic501865h | *Inorg. Chem.* XXXX, XXX, XXX−XXX

Table 1. Selected Bond Lengths (Å) and Angles (deg) for Compounds [1a]Cl·2H$_2$O, [1b](BF$_4$)·2H$_2$O, [1c](BF$_4$)·H$_2$O, [2c]Cl, {[4b](BF$_4$)(SiF$_6$)$_{0.5}$}·2H$_2$O, [5c](PF$_6$)$_2$·H$_2$O, and [7c]

distance/angle	[1a]Cl·2H$_2$O	[1b](BF$_4$)·2H$_2$O	[1c](BF$_4$)·H$_2$O	[2c]Cl
Ru1−Cl1	2.3851(8)	2.4068(16)	2.4105(12)	2.4047(12)
Ru1−N1(py)	2.093(2)	2.128(5)	2.108(3)	2.104(3)
Ru1−N2	2.075(2)	2.078(4)	2.078(4)	2.078(3)
N2−C6	1.319(3)	1.316(7)	1.321(5)	1.334(5)
N3−C6	1.341(4)	1.361(7)	1.346(6)	1.351(5)
N2−Ru1−N1	76.64(9)	76.56(18)	76.52(13)	75.85(12)
N1−Ru1−Cl1	85.25(6)	85.55(13)	84.69(10)	85.13(9)
N2−Ru1−Cl1	85.55(6)	84.74(13)	83.24(10)	84.20(9)

distance/angle	{[4b](BF$_4$)(SiF$_6$)$_{0.5}$}·2(H$_2$O)	distance/angle	[5c](PF$_6$)$_2$·H$_2$O	distance/angle	[7c]
Ru1−O1	2.124(3)	Ru1−N1(9-MeG)	2.134(3)	Ru1−Cl1	2.4251(8)
Ru1−N1(py)	2.132(4)	Ru1−N8(py)	2.135(4)	Ru1−C13	2.072(2)
Ru1−N2	2.070(4)	Ru1−N6	2.077(3)	Ru1−N1	2.0957(18)
N2−C6	1.333(6)	N6−C7	1.328(5)	N1−C7	1.332(3)
N3−C6	1.336(6)	N7−C7	1.341(5)	N2−C7	1.350(3)
N2−Ru1−N1	76.79(16)	N6−Ru1−N8	76.12(13)	C13−Ru1−N1	77.46(8)
N1−Ru1−O1	82.14(16)	N1−Ru1−N8	89.07(12)	C13−Ru1−Cl1	86.66(6)
N2−Ru1−O1	82.61(15)	N6−Ru1−N1	85.66(12)	N1−Ru1−Cl1	86.75(5)

deprotonation of the −NH group. Besides, the peaks attributed to L^1 in [**6b**] and [**6c**] are more shielded compared to those of HL^1 in the respective precursors [**1a**]**Cl** and [**1b**]**Cl** because of the anionic nature of L^1. The arene resonances of these neutral complexes are also upfield-shifted with respect to those of their monocationic precursors, in agreement with the general trend for cationic and neutral ruthenium(II) arene complexes.[22]

Finally, the ^{1}H NMR spectrum of the cyclometalated complex [(η^6-*p*-cym)RuCl(κ^2-*N*,*C*-L^4)] ([**7c**]) exhibits three well-defined ABCD spin systems for the aromatic protons of the deprotonated phenyl ring, the benzimidazole heterocycle, and the *p*-cym ligand. This characteristic pattern is in agreement with the formation of a cyclometalated complex with a κ^2-C,N chelate ring. Interestingly, the evolution with time of the corresponding NMR sample showed the slow rise of a second set of signals assigned to the Cl/DMSO-d_6 substitution product, with a molar ratio 56:44 for the equilibrium mixture after 5 days (see Figure 1SI-b in the SI).

On the other hand, the ^{13}C{^{1}H} NMR spectra recorded for some complexes show the expected signals for both the arene and aryldiazole ligands and exhibit symmetry patterns entirely consistent with those established by ^{1}H NMR (see the Experimental Section). In the case of [**7c**], a highly deshielded singlet attributed to the orthometalated C was recorded at 177.53 ppm, while the signal for the other *o*-C of the cyclometalated phenyl group was located at 123.64 ppm, which is almost 54 ppm upfield-shifted with regard to the former. This is consistent with the literature data.[19]

The FAB$^+$ mass spectra of the new compounds exhibit characteristic sets of peaks for different fragments: [M − Y]$^+$ for the monocationic complexes of the type [(η^6-arene)RuCl(κ^2-*N*,*N*-HL)]Y, fragments with one coordinated H$_2$O molecule for the aqua complexes described above; [M − 2PF$_6$ − H]$^+$ for [**5c**](**PF$_6$**)$_2$; [M + H]$^+$ for the neutral complexes [**6b**] and [**6c**], and [M]$^+$ for [**7c**].

The Fourier transform infrared spectra of all of the compounds, except those of the Cl$^-$ salts, exhibit strong diagnostic absorptions for the respective counteranions (see the Experimental Section).

The molar conductivity measurements (Λ_M) for the new compounds in aqueous solutions (10^{-3} M) confirmed the 1:1 electrolyte nature of the salts of monocationic complexes, the 1:2 electrolyte behavior of the salts of dicationic derivatives, and the molecular character of complex [**6c**] (Λ_M of complexes [**6b**] and [**7c**] could not be measured because of solubility difficulties (see the Experimental Section). However, the values measured for the neutral and monocationic species were slightly higher than expected, in agreement with partial dissociation of the chloride anion in water at room temperature (aquation).

Elemental analysis of the aqua compounds [**4a**](**BF$_4$**)$_2$, [**4b**](**BF$_4$**)$_2$, and [**4c**](**BF$_4$**)$_2$ did not acceptably match with the expected values as a result of presumable contamination with AgBF$_4$, and consequently these compounds were ruled out for biological studies.

X-ray Diffraction. Single crystals suitable for X-ray diffraction analysis were obtained for [**1a**]**Cl·2H$_2$O**, [**1b**]-(**BF$_4$**)·2H$_2$O, [**1c**](**BF$_4$**)·H$_2$O, [**2c**]**Cl**, {[**4b**](**BF$_4$**)(**SiF$_6$**)$_{0.5}$}·2H$_2$O (see the explanation below for the presence of SiF$_6^-$ as the counterion of [**4b**]$^{2+}$), [**5c**](**PF$_6$**)$_2$·H$_2$O, and [**7c**]. The ORTEP diagrams are shown in Figure 3, whereas selected bond lengths and angles with estimated standard deviations are gathered in Table 1, and relevant crystallographic parameters are given in the SI (Table 2SI-a,b). In all cases, the corresponding unit cells show the two possible enantiomers (R_{Ru} and S_{Ru}) resulting from the stereogenic nature of the metal center. All of the complexes adopt the classical pseudooctahedral three-legged piano-stool arrangement and, hence, the arene rings display the common π-bonded η^6-coordination mode, whereas the arylbenzimidazole-type ligands assume a bidentate-chelate coordination mode (κ^2-N,N or κ^2-C,N), occupying two coordination positions. The last place in the coordination sphere is occupied by a chloride ion, a H$_2$O molecule, or 9-MeG. In all of the derivatives, the structural features are comparable with those of similar compounds (see below).[23] The Ru−centroid distances for the different complexes fall in a narrow interval (1.667−1.697 Å) and are standard compared to alike complexes (Table 3SI in the SI).

The Ru−Cl bond distances in [**1a**]**Cl**, [**1b**](**BF$_4$**), [**1c**](**BF$_4$**), [**2c**]**Cl**, and [**7c**] are in the usual range, although the value for [**7c**] is shifted toward the upper limit [2.4251(8) Å], as in other cycloruthenated congeners,[7a,19] probably because of the

dx.doi.org/10.1021/ic501865h | Inorg. Chem. XXXX, XXX, XXX−XXX

Table 2. Solubility Data[a] in Water and the Aquation−Anation Ratio at Different NaCl Concentrations for Selected Compounds, Expressed as a Percentage of the Aqua Derivative in the Respective Equilibrium Mixture of Ru−OH_2 and Ru−Cl Complexes in D_2O (3 mM, Referring to the Initial Concentration of the Indicated Compound)[b]

			% aquation		
ref	compound	solubility (mM)	0 mM NaCl	5 mM NaCl	100 mM NaCl
[**1a**](**BF$_4$**)	[(phoxet)RuCl(HL^1)](BF$_4$)	2.9	74	50	9
[**1b**](**BF$_4$**)	[(bz)RuCl(HL^1)](BF$_4$)	5.9	69	49	9
[**1c**](**BF$_4$**)	[(*p*-cym)RuCl(HL^1)]BF$_4$	6.5	60	41	9
[**1a**]**Cl**	[(phoxet)RuCl(HL^1)]Cl	4.3	65	44	14
[**1b**]**Cl**	[(bz)RuCl(HL^1)]Cl	10.5	54	41	14.
[**1c**]**Cl**	[(*p*-cym)RuCl(HL^1)]Cl	141.2	52	44	11
[**2c**]**Cl**	[(*p*-cym)RuCl(HL^2)]Cl	37.0	49	35	12
[**3c**]**Cl**	[(*p*-cym)RuCl(HL^3)]Cl	157.5	59	45	12
[**4c**](**TfO**)$_2$	[(cym)Ru(OH$_2$)(2-pybzIm)](TfO)$_2$	27.5	100	65	13
[**6c**]	[(*p*-cym)RuCl(L^1)]	3.0	94	86	31
[**7c**]	[(*p*-cym)RuCl(L^4)]	NS	low solubility in water	low solubility in water	low solubility in water

[a]Solubility in water at room temperature (between 19 and 21 °C). [b]Data obtained from the ^{1}H NMR spectra recorded at 25 °C, in the absence of NaCl and then in the presence of either 5 or 100 mM NaCl solutions, by integration of the H$^{6'}$ signals.

concurrence of a second anionic ligand in the metal environment, namely, the strongly σ-donor ligand L^4.

The Ru−N distances are shorter for the benzimidazole heterocycle than for the pyridyl moiety in all of the cationic complexes with HL^1 and HL^2, that is, [**1a**]**Cl**, [**1b**](**BF$_4$**), [**1c**](**BF$_4$**), [**2c**]**Cl**, {[**4b**]$_2$(**BF$_4$**)$_2$(**SiF$_6$**)}, and [**5c**](**PF$_6$**)$_2$. In the case of [**7c**], the Ru−N(benzimidazole) bond [Ru1−N1 = 2.0957(18) Å] is considerably longer than those for the aforementioned cationic derivatives with HL^1 or HL^2. Besides, the orthometalated Ru−C distance [Ru1−C13 = 2.072(2) Å] is shorter than Ru1−N1 and also shorter than the Ru−N(py) bonds in its cationic relatives (Table 1) but similar to the Ru−C distances of related complexes. These features result from the strong σ-donor nature of the negatively charged C atom.[19b]

The N−Ru−X (X = N or C) angles of the chelate rings are determined by the features of the corresponding free bidentate ligands. These angles are very similar for all of the arylbenzimidazoles used in this work, with values between 76.12(13)° and 76.8(2)° for the complexes with HL^1 and values of 75.85(12)° and 77.46(8)° for the compounds [**2c**]**Cl**, and [**7c**], respectively. Some other geometrical parameters are gathered in Table 3SI in the SI and are briefly discussed there.

The compounds [**1a**]**Cl**, [**1b**](**BF$_4$**), and [**1c**](**BF$_4$**) exhibit a H_2O molecule in the second coordination sphere, linked to the N−H group of HL^1 through a strong hydrogen bond (N−H---O). A similar interaction has been reported for [η^5-CpRu(HL^1)(PPh$_3$)](PF$_6$).[24]

Furthermore, in the case of [**5c**](**PF$_6$**)$_2$, the O atom of 9-MeG is oriented toward the pyridyl moiety of HL^1 and takes part in a triple hydrogen-bonding interaction as an acceptor. Two of these contacts are intramolecular in nature: C21−H21---O1 with the *p*-cym ring and C18−H18---O1 with the pyridyl group (see Table 8SI and Figure 10SI in the SI); hence, these interactions reinforce the link between the nucleobase and the [(*p*-cym)Ru(HL^1)]$^{2+}$ fragment and could render the bonding selective to guanine relative to adenine, for instance. Sadler et al. have reported similar features in the specific recognition of DNA by complexes such as [(η^6-arene)Ru(9-EtG)(bpy(OH)O)]$^+$ [bipy(OH)O = deprotonated 2,2′-bipyridine-3,3′-diol][25] or [(η^6-arene)Ru(9-EtG)(en)]$^{2+}$ (en = $H_2NCH_2CH_2NH_2$) and [(η^6-arene)Ru(9-EtG)(Et-en)]$^{2+}$ [Et-en = Et(H)NCH$_2$CH$_2$NH$_2$].[26] In addition, there is a strong intermolecular hydrogen bond with a solvation H_2O molecule, O2−H(1O2)---O1 (Table 8SI and Figure 10SI in the SI). The 3D crystal architectures of the seven new compounds are built on the basis of hydrogen bonds, CH−π interactions, and π−π-stacking interactions (see the SI for a brief discussion of the intermolecular interactions of some compounds, as well as Tables 4SI−10SI and Figures 5SI−12SI).

Aqueous Solubility, Aquation−Anation Equilibria, and Hydrolysis Phenomena. *Solubility.* The aqueous solubility of the free ligands and some of the new compounds has been determined at room temperature (19−21 °C). The free ligands are not soluble in water, most likely because of strong self-association by hydrogen bonding and π−π-stacking interactions. By contrast, all of the studied compounds, except [**7c**], are soluble in water, although they exhibit solubility values in a broad range, 2.9−157.5 mM (Table 2). The enhanced solubility of the compounds relative to the free ligands is attributable to the blocking of the hydrogen-bonding acceptor atoms of the ligands (N atoms) after coordination and, in the cationic complexes, to the cation−cation repulsion, as well as the anion interposition, all of which contribute to disruption of the intermolecular hydrogen bonds that build the strong self-association in the crystal network of the free ligands.[27] Nevertheless, the solubility values show a strong dependence on the counterion, the overall charge of the complex (related to the formal charge of the ligands) and the arene identity. The chloride salts are much more soluble in water than their BF_4^- counterparts, in agreement with the trend observed in the literature for other families of ruthenium(II) arene complexes, which is explained as a result of the high hydration energy attributed to the Cl^- anion.[28] With regard to the arene influence, the *p*-cym derivatives give better solubilities than the bz and phoxet analogues. Within the *p*-cym series, the solubility diminishes according to the sequence [**3c**]**Cl** > [**1c**]**Cl** > [**2c**]**Cl** > [**4c**](**TfO**)$_2$ > [**6c**], indicating that substitution of HL^1 by HL^3 enhances the solubility in water because of the lower hydrophobicity of HL^3, whereas replacement of HL^1 by HL^2 produces the reverse result thanks to the presence of the less polar N−Me group in the benzimidazole heterocycle instead of the N−H unit. The aqua compound [**4c**](**TfO**)$_2$ only displays a modest ability to dissolve in water despite its dicationic nature, possibly by virtue of the limited hydrophilicity of TfO^-, and finally [**6c**] shows very poor solubility owing to their neutral nature. In particular, [**1c**]**Cl** and [**3c**]**Cl**

dx.doi.org/10.1021/ic501865h | Inorg. Chem. XXXX, XXX, XXX−XXX

Table 3. IC_{50} (μM, 96 h, 37 °C)[a] Values for Ligands HL^1, HL^2, HL^3, and HL^4 and Selected Compounds in the Cell Lines A2780, A2780cis, MCF-7, and MRC-5

							SF[c]		
ref	compound	A2780	A2780cis	RF[b]	MCF-7	MRC-5	A2780	A2780cis	MCF-7
	cisplatin	0.87 ± 0.01	5.17 ± 0.11	5.94	12 ± 1	4.87 ± 0.07	5.6	0.9	0.4
	HL^1	>100							
	HL^2	>100							
	HL^3	>100							
	HL^4	>100							
	$[(p\text{-cym})RuCl_2]_2$	>300[d]			>300[d]				
[1a]Cl	[(phoxet)RuCl(HL^1)]Cl	149 ± 3			66 ± 3				
[1b]Cl	[(bz)RuCl(HL^1)]Cl	96 ± 1			110 ± 6				
[1c]Cl	[(*p*-cym)RuCl(HL^1)]Cl	30 ± 1	34 ± 1	1.13	68 ± 1	224 ± 20	7.5	6.6	3.3
[1c](BF_4)	[(*p*-cym)RuCl(HL^1]BF_4	29 ± 1			68 ± 3				
[2c]Cl	[(*p*-cym)RuCl(HL^2)]Cl	35 ± 2	10 ± 2	0.29	29 ± 1	55 ± 4	1.6	5.5	1.9
[3c]Cl	[(*p*-cym)RuCl(HL^3)]Cl	19 ± 1	16 ± 1	0.84	38 ± 1	25 ± 1	1.3	1.6	0.7
[6c]	[(*p*-cym)RuCl(L^1)]	33 ± 2	30 ± 1	0.91			4.15	4.6	1.7
[7c]	[(*p*-cym)RuCl(L^4)]	11 ± 1	11 ± 1	1.00	26 ± 3[e]	34 ± 1	3.09	3.1	1.3

[a]The IC_{50} values are expressed as mean ± standard deviation from at least three independent experiments, as obtained by the MTT assay using exposure times of 96 h at 37 °C. [b]RF (resistance factor) = ratio of IC_{50} for A2780cis/IC_{50} for A2780; the lower the RF value, the better. [c]SF (selectivity factor) = ratio of IC_{50} for MRC-5/IC_{50} for either A2780 or MCF-7. MRC-5 fibroblasts are usually chosen as models for health cells to evaluate the selectivity of chemotherapeutic drugs.[33c] The higher the SF value, the more selective the activity. [d]Bibliography data: see refs in the text (incubation time = 72 h). [e][7c] has been tested to the highest possible concentration because interferences are observed at higher concentrations because of the characteristic color of this compound. Stock solutions of [7c] in DMSO were used, so the activity can be attributed to the equilibrium mixture between both [7c] and the Cl^-/DMSO substitution product.

exhibit exceptionally high solubility values. In any event, with the exception of [7c], all of the compounds are sufficiently soluble to enable biological studies in aqueous media and could circumvent hypothetical administration problems. Consequently, no correlation could be found between the solubility of the new compounds and the IC_{50} values (vide infra).

Hydrolysis. The $^{19}F\{^1H\}$ NMR spectra of the aqua derivatives $[\mathbf{4a}](\mathbf{BF_4})_2$, $[\mathbf{4b}](\mathbf{BF_4})_2$, and $[\mathbf{4c}](\mathbf{BF_4})_2$ in D_2O showed evidence of slow hydrolysis of the BF_4^- counterions at 5 °C (NMR sample kept in the refrigerator). In particular, two new resonances (A and B in Figure 4SI in the SI), apart from those for BF_4^-, were observed in the $^{19}F\{^1H\}$ NMR spectrum of $[\mathbf{4b}](\mathbf{BF_4})_2$ with molar ratios (A:B:BF_4^-) of 4:1:95 after 15 days and 24:17:59 after 60 days, respectively. The signal B at −144.1 ppm [1:1:1:1 quartet, $^1J(^{11}B-^{19}F)$ = 14.7 Hz], was attributed to $BF_3(OD)^-$ according to the literature.[29] Indeed, the slight tendency toward hydrolysis of BF_4^- in acidic media to produce HF and fluoroborates $[BF_{4-n}(OH)_n]^-$ (n = 1−4) is well documented[29] and in our case seems to be favored or catalyzed by the acidity of the ruthenium-coordinated ligand HL^1. The second resonance (A) at −130.45 ppm (s) was ascribed to SiF_6^{2-},[30] which is likely formed from the reaction between DF (HF) and the borosilicate glass of the NMR tube (see Figure 4SI in the SI and the equations therein). Consistently, a single crystal was obtained from the above-mentioned NMR sample of $[\mathbf{4b}](\mathbf{BF_4})_2$ in D_2O 3 months after its preparation, and the corresponding X-ray diffraction analysis confirmed cocrystallization of both counteranions BF_4^- and SiF_6^{2-}, along with the dicationic aqua complex $[\mathbf{4b}]^{2+}$ (see the structure above).

Aquation−Anation Equilibria. The aquation−anation equilibria of selected complexes were studied under pseudopharmacological conditions by recording the corresponding ^1H NMR spectra of 3 mM solutions in D_2O at 25 °C, in the absence of NaCl and afterward in the presence of NaCl (5 or 100 mM as model concentrations for the intracellular and blood plasma conditions, respectively). Signals for two different products were observed in all cases, and the molar ratio between them remained constant in the spectra recorded after 15 min and 1 h as evidence of fast equilibration. In particular, the two doublets appearing in each case at the highest frequencies were ascribed to the $H^{6'}$ protons of the aqua derivative (9.69−9.62 ppm) and its chlorido precursor (9.56−9.48 ppm; see Scheme 1 for numbering) and used as references for integration purposes. Consistently, the peak intensity of the chlorido species increased after the addition of NaCl, whereas a concomitant decrease in the peak intensity of the aqua species was observed. The aquation degree is expressed in every case as a percentage of the aqua complex in the equilibrium mixture (Table 2). An analysis of the data has allowed us to conclude that in the absence of NaCl all of the monocationic complexes undergo aquation to a notable extent, from 49 to 74%, with some differences depending on the counterion, the arene, or the bidentate aryldiazole ligand. In the presence of NaCl, all of the equilibria are shifted to the chlorido side with very similar aquation values for the different species, between moderate (in the presence of 5 mM NaCl) and low (in the presence of 100 mM NaCl), suggesting that, under these conditions, the effect of the counterion, the arene, or the pyridyldiazole ligand over dissociation of the chloride group is small. In addition, aquation of the neutral complex [6c] is the highest, 85.5% at 5 mM NaCl and even 30.6% at 100 mM NaCl. Surely, this is due to the high σ-donor character of its anionic ligand (L^1), which must favor dissociation of the chloride group. The formation of the more reactive aqua derivatives from their respective chlorido precursors is assumed to be the activation step for subsequent interaction with biological targets such as DNA or proteins, and so the reactivity tendencies of these complexes could explain, in part, their biological activity in some cases.

Antiproliferative Activity. The antiproliferative activity of the ligands HL^1, HL^2, and HL^3 and the proligand HL^4 and those of selected compounds has been evaluated in a

dx.doi.org/10.1021/ic501865h | Inorg. Chem. XXXX, XXX, XXX−XXX

comparative in vitro MTT cell viability assay after incubation times of 96 h at 37 °C with human ovarian carcinoma cells (A2780), cisplatin-resistant human ovarian carcinoma cells (A2780cis), and human hormone-dependent breast cancer cells (MCF-7). The activity values, summarized in Table 3, are expressed as the inhibitory potency (IC_{50}). Cisplatin was used as the positive control in all of the cell lines. The cytotoxicity of the free ligands is very low (IC_{50} > 100 μM) in the chemosensitive A2780 cell line, and for this reason, it was not tested in the A2780cis or MCF-7 cells. Likewise, the dimeric starting material $[Ru(p\text{-cym})Cl_2]_2$ is inactive in these cell lines according to the literature data.[31] By contrast, most of the new ruthenium compounds evaluated in the cell line A2780 showed moderate or good activity. Thus, the most prominent in vitro inhibitory potencies were obtained for the neutral cyclometalated complex [**7c**] (IC_{50} = 11 ± 1 μM) and the monocationic derivative [**3c**]**Cl** (IC_{50} = 19 ± 1 μM). Both results compare reasonably well with other notably cytotoxic ruthenium(II) arene derivatives reported recently.[6d,22,32] In the MCF-7 cells, the best results were achieved for [**7c**] (IC_{50} = 26 ± 3 μM), [**2c**]**Cl** (IC_{50} = 29 ± 1 μM), and [**3c**]**Cl** (IC_{50} = 38 ± 1 μM), which are only between 2- and 3-fold less active than cisplatin. Nevertheless, the remainder of the compounds exhibited a low performance in this cell line compared to other ruthenium(II) complexes.[33] The antiproliferative activity of compounds [**2c**]**Cl** and [**3c**]**Cl** toward the A2780cis cells is unusual as long as the corresponding IC_{50} values are lower than those for the A2780 cells. Thus, the resistance factor, RF, for these compounds is below unity, indicating that [**2c**]**Cl** and [**3c**]**Cl** overcome cisplatin resistance. Finally, the selectivity factors (SF = IC_{50} for MRC-5/IC_{50} for the respective cancer cells) have been determined for some compounds, as a measure of the tumor-selective antiproliferative potency. The MRC-5 normal fibroblasts are usually chosen as models for healthy cells in this kind of analysis. In this regard, the most prominent drug turned out to be [**1c**]**Cl** because of the low cytotoxicity of this compound toward the fibroblasts. Thus, the SF values for [**1c**]**Cl** are higher than those of cisplatin in the three cancer cell lines—7.5 versus 5.6 (A2780); 3.3 versus 0.4 (MCF-7) and 6.6 versus 0.9 (A2780cis)—and this compound can be postulated as a clinical alternative in the treatment of ovarian cancer on the basis of this result.

Furthermore, a comparison of the IC_{50} values obtained for [**1a**]**Cl**, [**1b**]**Cl**, and [**1c**]**Cl** in the A2780 and MCF-7 cells (Table 3) suggests that the arene ring affects the cytotoxic activity. In both cell lines, [**1c**]**Cl** with *p*-cym is more active than [**1b**]**Cl** with bz. Compound [**1a**]**Cl** shows erratic behavior because it is the less active compound in the A2780 cells but exhibits an activity similar to that of [**1c**]**Cl** in the MCF-7 cells.

As a matter of fact, the arene group is known to have a crucial effect on the cytotoxicity.[34] Among the main arene features, modulation of the aquation rate and the influence on the acidity constants of Ru-aqua species stand out. Both effects are directly related to the biological activity of the ruthenium compounds because the aqua species are the biologically active species.[35] Moreover, the arene type affects the coordination rate of the Ru center to the guanine N7 site, with complexes containing an extended arene being faster than those containing a monoarene group.[36] In fact, complexes endowed with an extended arene are able to interact with DNA by both covalent binding and intercalation of the arene moiety.[37] Furthermore, the cytotoxic activity in A2780 cancer cells has been shown to increase with the size of the coordinated arene: bz < *p*-cym < biphenyl < dihydroanthracene < tetrahydroanthracene.[38] To shed light on the mechanism of the cytotoxic activity of compounds [**1a**]**Cl**, [**1b**]**Cl**, and [**1c**]**Cl**, the acid-dissociation constant (pK_a), the rate of aquation, and the DNA binding ability were assessed, analyzing if these properties are affected by the arene identity or bear some relationship with their relative biological activity.

Determination of the pK_a Values of HL^1, [1a]Cl, [1b]Cl, and [1c]Cl. The acid-dissociation constants, pK_a, were determined by recording the absorbance spectra of the free ligand HL^1 and the ruthenium compounds [**1a**]**Cl**, [**1b**]**Cl**, and [**1c**]**Cl**. Figure 13SIA in the SI shows the UV−vis absorbance spectrum of HL^1, and Figure 13SIB in the SI the absorbance data at 335 nm and different acidity levels; the data pairs were analyzed with eq 5SI in the SI.

Table 4 lists the pK_a values of HL^1 at 5 mM NaCl. The three different species involved in the ionization equilibria of the free ligand are the monocationic species ($[H_2L^1]^+$) with the pyridyl N site protonated (prevailing at pH < 4.06), the neutral species (HL^1) predominant from pH ≥ 4.06 to pH ≤ 12.50, and the anionic species ($[L^1]^-$) resulting from deprotonation at the benzimidazole N site (prevailing at pH >12.50). The deprotonation scheme is depicted in Figure 14SI in the SI.

Table 4. pK_a Values Obtained for HL^1, [1a]Cl, [1b]Cl, and [1c]Cl at Different Ionic Strengths

compound	[NaCl], mM	pK_{a1}	pK_{a2}
HL^1	5	4.06 ± 0.02	>12.50
[**1a**]**Cl**	5	6.11 ± 0.02	8.56 ± 0.05
	100	6.73 ± 0.01	8.84 ± 0.04
	500	6.87 ± 0.02	9.22 ± 0.04
[**1b**]**Cl**	5	6.11 ± 0.02	8.56 ± 0.01
[**1c**]**Cl**	5	6.07 ± 0.04	8.97 ± 0.04

As for ionization of the ruthenium complexes, because of the close similarity of the UV−vis spectra, only that of [**1b**]**Cl** is shown (Figure 15SI in the SI). The presence of several isosbestic points unveils different species in equilibrium. The absorbance (at 344 and 353 nm) versus the pH plot reveals two different equilibria, providing the acidity constants by means of eq 5SI in the SI. Table 4 lists the pK_a values at different ionic strengths; these results correlate well with those reported for other ruthenium complexes containing HL^1.[39] Hence, three species can be set for the ruthenium complexes: the monocationic species (prevailing at pH <6), the neutral species resulting from N−H deprotonation (prevailing in the 6 ≤ pH ≤ 9 range), and presumably the neutral hydroxido species (pH >9) (Figure 4).

Therefore, the pK_a value for deprotonation of the N−H group in HL^1 dramatically dropped from 12.5 to 6.1 as a result of coordination. In summary, at pH 7.0, where the DNA binding has been studied, the ruthenium(II) complexes are present in the chlorido neutral form. To check whether formation of the hydroxo species is possible without the involvement of the aqua complex, the equilibrium constants of [**1a**]**Cl** were evaluated at different NaCl concentrations, I = 5, 100, and 500 mM. Inspection of Table 2 reveals that a percentage of the aqua complex strongly diminished upon an increase in the salt content. For I = 0.5 M, only the chloro complex was detected (result not shown). The spectrophotometric behavior for all ionic strenghts was similar to that of Figure 15SI in the SI, and we can conclude that involvement of the aqua complex intermediate in the formation of the hydroxo

dx.doi.org/10.1021/ic501865h | *Inorg. Chem.* XXXX, XXX, XXX−XXX

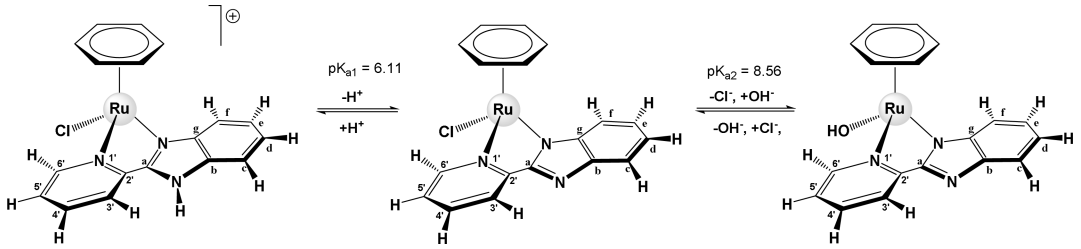

Figure 4. Dissociation equilibria for [**1b**]Cl.

Table 5. Rate Constants Obtained for Aquation (k_{aq}) and Covalent Binding (k_{cb}) of [1a]Cl, [1b]Cl, and [1c]Cl Alone and in the Presence of 5′-dGMP and CT-DNA[a]

	alone	5′-dGMP		CT-DNA	
	10^4k_{aq}	10^3k_{aq}	10^4k_{cb}	10^3k_{aq}	10^5k_{cb}
[**1a**]Cl	3.2 ± 0.02	2.5 ± 0.1	3.5 ± 0.1	2.2 ± 0.1	7.0 ± 0.1
[**1b**]Cl	4.6 ± 0.03	1.4 ± 0.1	1.3 ± 0.1	1.1 ± 0.3	3.2 ± 0.2
[**1c**]Cl	11.9 ± 0.04	7.2 ± 0.1	5.1 ± 0.1	4.3 ± 0.2	9.0 ± 0.1

[a] $C_D = 3.6 \times 10^{-5}$ M, $C_P/C_D = 10$, pH 7.0, $I = 5$ mM (NaCl), and $T = 25$ °C. C_D stands for the ruthenium compound concentration, and C_P stands for the concentration of 5′-dGMP or CT-DNA.

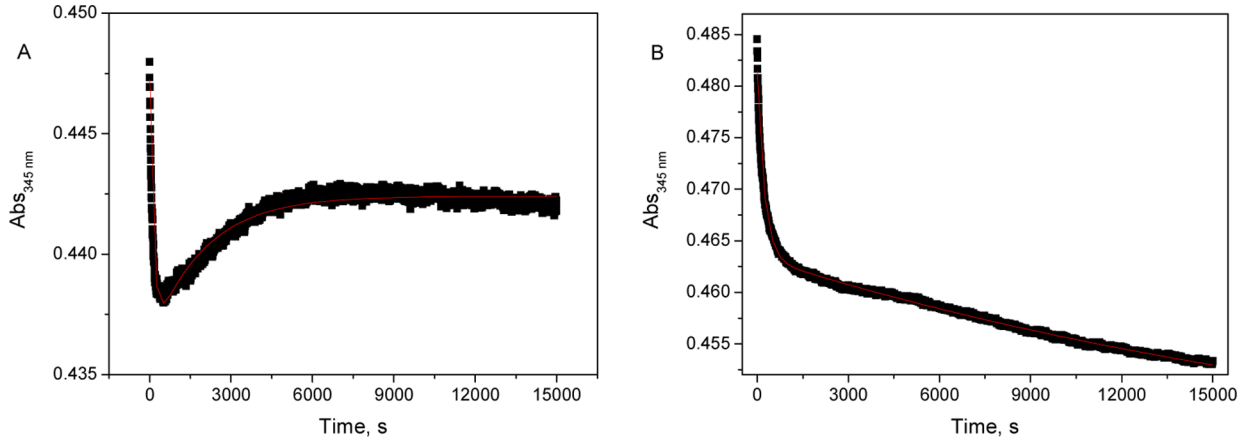

Figure 5. Absorbance/time kinetic curve and fitting by a biexponential function (red line) for the 5′-dGMP/[**1a**]Cl system (A) and for the CT-DNA/[**1c**]Cl system recorded at $\lambda = 345$ nm, $C_D = 3.6 \times 10^{-5}$ M, $C_P/C_D = 10$, pH 7.0, $I = 5$ mM (NaCl), and $T = 25$ °C.

complex can be discarded. At the same 5 mM ionic strength, the data of Table 4 show that pK_{a1} is independent of the arene substituent, whereas pK_{a2} is higher for [**1c**]Cl than for [**1a**]Cl and [**1b**]Cl. The greater antiproliferative activity of [**1c**]Cl could be related to the lower reactivity of the Ru−OH derivative.[7a]

Determination of the Aquation Rate Constants for [1a]Cl, [1b]Cl, and [1c]Cl. A kinetic study of the aquation process (formation of H_2O−Ru) of the [**1a**]Cl, [**1b**]Cl, and [**1c**]Cl compounds was carried out spectrophotometrically at I = 5 mM (NaCl) and pH 7.0.

Figure 16SI in the SI shows the kinetic curve corresponding to aquation of [**1b**]Cl alone, and Table 5 lists the aquation rate constants (k_{aq}) for the three systems alone, with values in the sequence [**1a**]Cl < [**1b**]Cl < [**1c**]Cl. The k_{aq} value for [**1c**]Cl was almost 4 and 3 times higher than those of [**1a**]Cl and [**1b**]Cl, respectively. Therefore, as reported earlier,[35] it is plausible to link the observed higher activity of [**1c**]Cl with the aquation rate constant.

Binding of [1a]Cl, [1b]Cl, and [1c]Cl with the Mononucleotide 5′dGMP and CT-DNA. Kinetic, Circular Dichroism, and Melting Temperature. The covalent binding between ruthenium(II) of [**5c**](**PF$_6$**)$_2$ and 9-MeG has been structurally supported by X-ray diffraction (Figure 3). However, to ensure that the Ru^{II}−N7G bond is also formed in aqueous solution DNA-containing complexes, a kinetic study of the reaction of the compounds [**1a**]Cl, [**1b**]Cl, and [**1c**]Cl with 5′dGMP and CT-DNA has been conducted spectrophotometrically. The kinetic runs were fitted to biexponential functions (Figure 5). Table 5 lists the results of the fitting and the k_{aq} and k_{cb} values obtained for 5′dGMP and CT-DNA under the same conditions in the three systems, with k_{aq} and k_{cb} being the rate constants of the aquation process (fast reaction) and formation of the Ru^{II}−N7G covalent binding (slow reaction), respectively. For the systems with [**1c**]Cl, the two constants were slightly bigger compared to those of [**1a**]Cl and [**1b**]Cl. The k_{aq} value in the presence of 5′dGMP and CT-DNA was almost 1 order of magnitude higher than that in their absence (Table 5); that is, the second reaction accelerates the aquation. The k_{cb} values in the presence of CT-DNA were smaller than those in the presence of 5′dGMP, indicating that the intercalation binding to DNA displayed by the benzoazole ligand (see below) obstructs the covalent binding.

dx.doi.org/10.1021/ic501865h | Inorg. Chem. XXXX, XXX, XXX−XXX

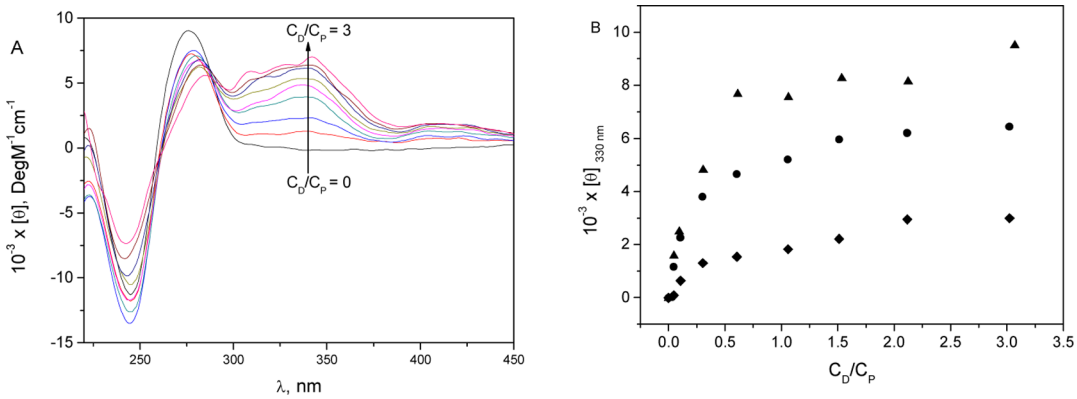

Figure 6. (A) CD spectra for the CT-DNA/[**1a**]**Cl** system. (B) Molar ellipticity at λ = 330 nm of (●) CT-DNA/[**1a**]**Cl**, (▲) CT-DNA/[**1b**]**Cl**, and (♦) CT-DNA/[**1c**]**Cl**. C_P= 5.1 × 10^{-5} M; C_D/C_P = 0–3.

Solutions containing different C_D/C_P ratios (P = DNA and D = [**1a**]**Cl**, [**1b**]**Cl**, and [**1c**]**Cl**) were incubated overnight. Thus, once the Ru^{II}–N7G covalent binding is formed, the structural changes were studied by circular dichroism (CD) and thermal denaturation measurements.

Figure 6A shows that positive bands emerged at 330 and 420 nm for both the DNA/[**1a**]**Cl** and DNA/[**1b**]**Cl** systems, whereas for the DNA/[**1c**]**Cl** system only the new band at 330 nm could be observed. In all cases, two isodichroic points appeared in the sets of CD curves. The compounds show bathochromic and hypochromic effects of the positive band of DNA (λ = 275 nm) as the C_D/C_P ratio was raised. This effect is more perceptible with [**1a**]**Cl** and [**1b**]**Cl** than with [**1c**]**Cl**. On the other hand, the 3 nm blue shift of the negative band of DNA at 245 nm was absent for DNA/[**1c**]**Cl**. These features are related to the different extent of intercalation.[40] Another interesting difference was found in the amplitude of the induced CD band at 330 nm, which for the DNA/[**1c**]**Cl** system was smaller compared with that for [**1a**]**Cl** or [**1b**]**Cl** (Figure 6B). Therefore, it seems evident that the *p*-cym arene prevents intercalation of the benzoazole ligand to a greater extent than bz and phoxet.

The melting experiments were carried out at different C_D/C_P ratios, and the values of the melting temperature, T_m, were calculated from the absorbance–temperature curves. Figure 7 shows the negative slope in the T_m versus C_D/C_P plot; from the negative slopes, we can infer a higher destabilizing effect on DNA for [**1c**]**Cl** compared to that for [**1a**]**Cl** and [**1b**]**Cl**, which shows little effect on the thermal stability of DNA; that is, the *p*-cym group destabilizes DNA to a greater extent than the bz and phoxet groups.

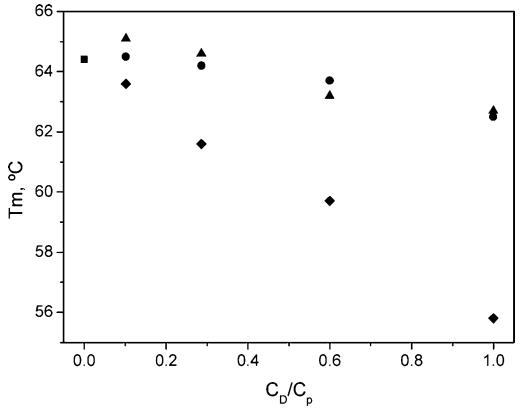

Figure 7. Melting temperature as a function of the C_D/C_P ratio of (■) DNA alone and the systems (●) DNA/[**1a**]**Cl**, (▲) DNA/[**1b**]**Cl**, and (♦) DNA/[**1c**]**Cl**. C_P = 4.1 × 10^{-5} M; C_D/C_P = 0–1, I = 5 mM (NaCl), C_P = 4.1 × 10^{-5} M, pH 7.0, temperature range from 35 to 95 °C; scan rate of 0.3 °C/min.

Intercalation of a dye into the base pairs of DNA causes a stabilizing effect of the double helix and, hence, the slope of the T_m versus C_D/C_P plot becomes more positive insofar as the intercalation extent of the drug increases.[41] On the other hand, the covalent binding of a complex to the helix destabilizes the double helix, resulting in a negative slope of the T_m versus C_D/C_P plot.[42] Given that both types of binding were present in all three complexes, [**1a**]**Cl**/CT-DNA, [**1b**]**Cl**/CT-DNA, and [**1c**]**Cl**/CT-DNA, it can be concluded that, for the latter, the destabilizing effect prevails because of the smaller intercalation occasioned by the influence of *p*-cym compared to bz and phoxet.

From the CD, melting, and aquation rate constant data gathered, it was verified that [**1c**]**Cl** manifests a well-differentiated behavior relative to [**1a**]**Cl** and [**1b**]**Cl**. Concerning this feature, the *p*-cym ring plays a positive role in the observed cytotoxicity for both A2780 and MCF-7 cells (vide supra) compared to bz. Hence, a direct relationship between the DNA–complex interaction and the biological activity can indeed be established.

In Vitro Inhibition of Cyclin-Dependent Kinase 1 (CDK1). The in vitro inhibitory ability of selected ligands and compounds toward the CDK1 activity was evaluated to shed light into a possible multitarget mechanism for the cytotoxic properties of these compounds. For comparison purposes, staurosporine was included in the assay. As shown in Table 6, the CDK1 inhibitory potency of the tested compounds is poor compared to that of the reference drug and other ruthenium(II) complexes.[43] However, it is worth mentioning here that HL^1 is the most active drug among the free ligands. Moreover, compounds [**1c**]**Cl**, [**4c**](**TfO**)$_2$, and [**6c**], all with HL^1, show higher activity relative to the free ligand and yield the best results among the studied ruthenium(II) derivatives. These data point to a synergistic effect on the CDK1 inhibition for the combination between HL^1 and the metal fragment [(η^6-*p*-cym)RuX]$^{n+}$. Moreover, these results, together with the ability of [**1c**]**Cl** to bind DNA, suggest a possible multitarget mechanism, at least for the antiproliferative activity of this compound.

dx.doi.org/10.1021/ic501865h | *Inorg. Chem.* XXXX, XXX, XXX–XXX

Table 6. Inhibition Values (%) of Selected Ligands and Compounds toward CDK1

ref	compound	% inhibition at 100 μM
	HL^1	24 ± 2
	HL^2	19 ± 1
	HL^3	3 ± 2
	HL^4	20 ± 1
[1c]Cl	[(*p*-cym)RuCl(HL^1)]Cl	45 ± 1
[2c]Cl	[(*p*-cym)RuCl(HL^2)]Cl	15 ± 1
[3c]Cl	[(*p*-cym)RuCl(HL^3)]Cl	12 ± 1
[4c](TfO)$_2$	[(*p*-cym)Ru(OH_2)(HL^1)](TfO)$_2$	51 ± 4
[6c]	[(*p*-cym)RuCl(L^1)]	49 ± 6
[7c]	[(*p*-cym)RuCl(L^4)]	25 ± 4

IC_{50}(staurosporine) = 15.33 nM.

SAR. The new complexes described in this work have been furnished with different motifs in their structural elements in order to gain a better understanding of the optimal features for antitumor activity. The following structure−property and structure−activity relationships are inferred primarily from the solubility of the different compounds in water and the cytotoxic potency of the different drugs in the chemoselective A2780 cell line, with some remarks regarding the MCF-7 cells (see Figure 8 for a graphical summary), as well as the aquation rate constants and DNA interaction studies.

(a) We have concluded that coordination of the aryl-substituted benzimidazole molecules to different [(arene)-RuX]$^+$ fragments has a beneficial influence on the anticancer activity of the resulting complexes compared to that of the free ligands or the dimeric starting materials, suggesting a synergistic effect for the combination of both elements in a single molecule. Moreover, this effect hints at a mechanism in which the metal site interacts with the biological target (allegedly DNA) promoted by the ligand.

(b) To a second place, **[1c]Cl** and **[1c](BF$_4$)** were found to be equally active in the two cell lines studied (A2780 and MCF-7), ruling out a counterion effect despite the small difference in the aqueous solubility of both salts and the slight tendency toward hydrolysis of the BF_4^- ion in an acidic medium. On the other hand, it is worth mentioning that, according to the literature, other counteranions with more lipophilic character, such as BPh_4^-, can modulate the cellular uptake of ruthenium-(II) cationic complexes by ion pairing.[44]

(c) The effect of the arene identity was evaluated from a comparison of the IC_{50} values of **[1a]Cl**, **[1b]Cl**, and **[1c]Cl**. Thus, the activity sequence in both cell lines (A2780 and MCF-7) turned out to be **[1c]Cl** > **[1b]Cl**, indicating that *p*-cym behaves better than bz. Regarding phoxet, the results are somehow contradictory because it shows a detrimental impact compared to *p*-cym over the inhibitory potency in the A2780 cells, whereas both IC_{50} values are very similar in the MCF-7 cells. The superior performance in the antiproliferative activity of *p*-cym-Ru^{II} derivatives over their bz counterparts has already been reported and attributed to the presence of electron-donor groups in the *p*-cym ring, which promote chloride dissociation.[32b,43] In our systems, this effect is also observed, but the higher destabilizing influence of **[1c]Cl** over the secondary structure of DNA could play an important role as well.

(d) The effect of the overall charge of the metal complex, the presence of the N−H group, or even the σ-donor ability of the ancillary ligand on the inhibitory concentration is difficult to establish, owing to the dependence of these structural features on the pH and Cl^- concentration. In the A2780 cells, the IC_{50} values for **[1c]Cl** and **[6c]** are very similar because **[6c]** is formally the conjugate base of **[1c]Cl**, and, consequently, the protonation state will depend only on the pH, regardless of the complex used in the in vitro assays. Indeed, complexes $[\mathbf{1c}]^+$, **[6c]**, and $[\mathbf{4c}]^{2+}$ can be seen as part of a system whose chemical and biological properties can be tuned through protonation/deprotonation and aquation/anation. Comparison of the IC_{50} values for **[6c]** and **[7c]** is also difficult to interpret for the same reason; that is, the actual protonation state of these species will depend on the above-mentioned external factors. Nevertheless, the IC_{50} value for **[7c]** is 3-fold lower than that for **[6c]** in the A2780 cells, although the low solubility of **[7c]** could remain as a limitation for further studies. Three similar ruthenium(II) complexes with funtionalized cyclometalated benzimidazole ligands have been reported recently, with IC_{50} values comparable to those of **[7c]** in the A2780 cells.[6d]

(e) The presence of the benzo ring in the diazole heterocycle seems to have a notorious negative effect on both the aqueous

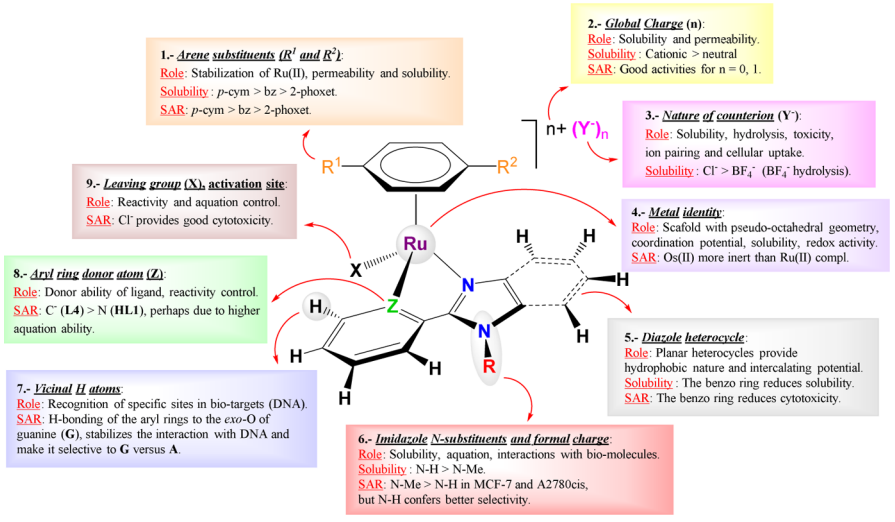

Figure 8. Graphical scheme showing the general role/function of different structural elements, the aqueous solubility, and the SAR based on the IC_{50} values for A2780, A2780cis, and MCF-7 for the present family of complexes.

dx.doi.org/10.1021/ic501865h | *Inorg. Chem.* XXXX, XXX, XXX−XXX

solubility and the inhibitory potency toward all of the cancer cells used in this study. In fact, [**3c**]**Cl** is more soluble in water than [**1c**]**Cl** and also more active in the three cancer cells utilized. Nevertheless, [**1c**]**Cl** exhibits better selectivity factors.

(f) Finally, replacement of the N−H group by a N−Me group in the aryldiazole ligand diminishes the solubility in water and confers a variable effect on the cytotoxic activity depending on the cancer cell line, as concluded from a comparison of the IC_{50} values of [**1c**]**Cl** and [**2c**]**Cl**. In particular, [**2c**]**Cl** provides a better IC_{50} value than [**1c**]**Cl** in the MCF-7 cells and shows potential to overcome the cisplatin resistance. However, [**1c**]**Cl** bestows better selectivity values than [**2c**]**Cl**.

Concluding Remarks. The HL^1, HL^2, and HL^3 ligands and the HL^4 proligand have been used to prepare an ample series of ruthenium(II) arene complexes, aiming to fine-tune the cytotoxic properties of these types of promising anticancer drugs. The crystal structure of seven of the new derivatives has been elucidated by X-ray diffraction. For the 9-MeG derivative, [**5c**]$(PF_6)_2$, subsequent structural analysis has provided critical information about intramolecular hydrogen-bonding interactions in the specific recognition of guanine (DNA) as a putative biological target. A selection of the new compounds has been assessed for their in vitro antiproliferative activity against A2780, A2780cis, and MCF-7 cells and MRC-5 fibroblasts, and detailed SAR about the key functional groups have been settled. Thus, the *p*-cym arene seems to improve the activity versus bz, whereas phoxet shows erratic behavior. Besides, positive effects on the cytotoxic activity are attributed to the presence of the N−Me group and the absence of the benzo ring in the benzoazole unit. Compounds [**1c**]**Cl**, [**2c**]**Cl**, [**3c**]**Cl**, [**6c**], and [**7c**] provided the best antiproliferative activity, deserving further study in different cell lines as potential anticancer drugs. Indeed, additional biological studies to determine the action mechanism and the actual target of [**7c**] and $[\mathbf{4c}]^{2+}$, as the active species of [**1c**]**Cl**, are ongoing nowadays in our laboratory and will be reported in due course. In addition, the three $[(\eta^6\text{-arene})RuCl(\kappa^2\text{-}N,N\text{-}HL^1)]Cl$ compounds differing in the arene moiety, studied in terms of DNA binding, suffered aquation at low ionic strength, I = 5 mM (NaCl), and displayed covalent binding in the presence of 5′-dGMP or CT-DNA. The formation rate constant of the Ru−N7 bond of the guanine residue is smaller with CT-DNA than with 5′-dGMP because in the former other noncovalent binding modes, such as intercalation of the ligand between the DNA base pairs, could occur, hindering the covalent binding. It can then be concluded that the three compounds studied here interact with DNA in a bifunctional way, involving covalent binding and intercalation. The type of arene plays a significant role in the DNA binding, as inferred from the collected results. Thus, the complex with *p*-cym displays the smallest intercalation degree compared to bz or phoxet and destabilizes the DNA structure more than the others.

EXPERIMENTAL SECTION

General Methods and Starting Materials. Starting materials: $RuCl_3{\cdot}xH_2O$ was purchased from Apollo Scientific Ltd. and used as received. $[(\eta^6\text{-arene})Ru(\mu\text{-}Cl)Cl]_2$ (arene = *p*-cym, bz,[45] or phoxet[46]) was prepared according to literature procedures. $AgBF_4$, the ligand 2-(2-pyridyl)benzimidazole (HL^1), and the proligand 2-phenylbenzimidazole (HL^4) were purchased from Aldrich and used without further purification. The ligands 1-methyl-2-pyridin-2-yl-1*H*-benzimidazole (HL^2)[47] and 2-(1*H*-imidazol-2-yl)pyridine (HL^3)[48] were prepared according to literature procedures. Deuterated solvents were obtained from SDS and Euriso-top. The aqueous solutions were prepared with doubly deionized water from a Millipore Q apparatus (APS; Los Angeles, CA). Calf-thymus DNA (CT-DNA) was purchased from Sigma-Aldrich as a lyophilized sodium salt, and DNA was dissolved in doubly deionized water and sonicated. The DNA sonication was carried out using a MSE-Sonyprep sonicator, by application to suitable CT-DNA samples (10 mL of CT-DNA of ca. 2×10^{-3} M_{BP}) seven repeated cycles of 10 s sonication and 20 s pause, at 14 μm amplitude. The sonicator tip was introduced directly into the solution and kept in an ice bath to minimize thermal effects due to sonication. The polynucleotide concentration, M_{BP}, is expressed in molarity of base pairs and denoted as C_P. The ionic strength was adjusted using sodium chloride, and sodium cacodylate, $(CH_3)_2AsO_2Na$, was used to keep the acidity constant at pH 7.0.

All synthetic manipulations were carried out under an atmosphere of dry, O-free N_2 using standard Schlenk techniques. The solvents were distilled from the appropriate drying agents and degassed before use. Elemental analyses were performed with a PerkinElmer 2400 CHN microanalyzer. The analytical data for the new compounds were obtained from crystalline samples when possible. In some cases, the data were totally accurate, but in others, the agreement of the calculated and found values for C was >0.4%, so that solvent molecules were introduced in the molecular formulas to improve agreement. IR spectra were recorded on a Nicolet Impact 410 spectrophotometer (4000−400 cm^{-1} range) as KBr pellets. FAB mass spectra (position of the peaks in DA) were recorded with an Autospec spectrometer. The isotopic distribution of the heaviest set of peaks matched very closely that calculated for the formulation of the complex cation in every case. NMR samples were prepared under a N_2 atmosphere by dissolving the suitable amount of compound in 0.5 mL of the respective oxygen-free deuterated solvent, and the spectra were recorded at 298 K (unless otherwise stated) on a Varian Unity Inova-400 (399.94 MHz for ^1H; 161.9 MHz for ^{31}P; 376.28 MHz for ^{19}F; 100.6 MHz for ^{13}C). Typically, 1D ^1H NMR spectra were acquired with 32 scans into 32K data points over a spectral width of 16 ppm. ^1H and $^{13}C\{^1H\}$ chemical shifts were internally referenced to tetramethylsilane via 1,4-dioxane in D_2O (δ = 3.75 and 67.19 ppm, respectively) or via the residual ^1H and ^{13}C signals of the corresponding solvents, CD_3OD (δ = 3.31 and 49.00 ppm) and $(CD_3)_2CO$ (δ = 2.05 and 29.84 ppm), according to the values reported by Fulmer et al.[49] Chemical shift values are reported in ppm and coupling constants (J) in hertz. The splitting of proton resonances in the reported ^1H NMR data is defined as s = singlet, d = doublet, t = triplet, st = pseudotriplet, q = quartet, sept = septet, m = multiplet, bs = broad singlet. All ^{31}P resonances were referenced against an external standard of 85% H_3PO_4 at 0 ppm. 2D NMR spectra such as $^1H-^1H$ gCOSY, $^1H-^1H$ NOESY, $^1H-^{13}C$ gHSQC, and $^1H-^{13}C$ gHMBC were recorded using standard pulse sequences. The probe temperature (±1 K) was controlled by a standard unit calibrated with methanol as a reference. All NMR data processing was carried out using *MestReNova*, version 6.1.1.

Characterization data have been moved to the SI.

The pH values of NMR samples in D_2O were measured at room temperature before and after recording the NMR spectra, using a Metrohm 16 DMS Titrino pH meter fitted with a combined glass electrode and a 3 M KCl solution as a liquid junction, which was calibrated with Radiometer Analytical SAS buffer solutions at pH 1.679, 2.000, 4.005, 6.865, 7.000, and 7.413. No correction was applied for the effect of deuterium on the glass electrode.

Spectrophotometric measurements and thermal denaturation experiments were performed on a Hewlett-Packard 8453A spectrophotometer (Agilent Technologies, Palo Alto, CA) fitted with diode-array detection and computer-assisted temperature control systems. The measurements were performed in a 1.0-cm-path-length cell. Thermal denaturation experiments were carried out at constant CT-DNA concentration ($C_P = 4 \times 10^{-5}$ M) and with variation of the C_D/C_P ratio from 0 to 1. The absorbance at 260 nm was recorded during the heating from 35 to 95 °C at a 0.3 °C/min scan rate with 1 min of stabilization time.

CD spectra were recorded on a MOS-450 Bio-Logic spectrometer (Claix, France). The measurements were performed in 1.0-cm-path-length cells at 25 °C. CD titrations have been carried out by adding

dx.doi.org/10.1021/ic501865h | *Inorg. Chem.* XXXX, XXX, XXX−XXX

increasing amounts of the ruthenium compounds into the cell containing the CT-DNA solution ($C_P = 5 \times 10^{-5}$ M), with variation of the C_D/C_P ratio from 0 to 3.

Cytotoxicity Assays in Cancer Cells. The MTT proliferation assay is based on the reduction of the yellow MTT tetrazolium salt (3-[4,5-dimethylthiazol-2-yl]-2,5diphenyltetrazolium bromide) by mitochondrial dehydrogenases to form a blue MTT formazan in viable cells.[50] Approximately 4×10^3 cells per well for both A2780 and A2780cis and 1×10^4 cells per well for either MCF-7 and MRC-5 were cultured in 100 μL of a growth medium in 96-well plates and incubated at 37 °C under a 5% CO_2 atmosphere. The growth media were RPMI 1640 with 10% fetal bovine serum (FBS) and 2 mM L-glutamine in a 95% air, 5% CO_2 atmosphere for A2780 and A2780cis cells, minimun essential medium eagle (EMEM) with 10% FBS in 95% air, 5% CO_2 atmosphere for MRC-5, and EMEM with 2 mM L-glutamine and Earle's BSS adjusted with 1.5 g/L $NaHCO_3$, 0.1 mM nonessential amino acids, and 1 mM sodium piruvate supplemented with 10% FBS and 0.01 mg/mL bovine insulin in a 95% air, 5% CO_2 atmosphere for MCF-7 cells. The cells were grown for 24 h, and the growth medium was replaced by a fresh medium containing different concentrations of the compounds to be assayed and maintained at 37 °C in a 5% CO_2 atmosphere for either 96 h (A2780, A2780cis, or MCF-7 cell lines) or 168 h (MRC-5 cell line). Cisplatin was used as a positive control. After this time, 10 μL of a 5 mg/mL solution of MTT in PBS (0.136 mM NaCl, 1.47 mM KH_2PO_4, 8 mM NaH_2PO_4, and 2.68 mM KCl) were added to each well, and the cells were maintained at 37 °C in a 5% CO_2 atmosphere for 4 h; afterward, 100 μL of a 10% SDS solution in 0.01 M HCl was added to each well, and the cells were maintained at 37 °C in a 5% CO_2 atmosphere for 12−14 h. Absorbance was read at λ = 595 nm in an Ultra-Evolution microplate reader (Tecan). At least two independent experiments were performed with three replicates per dose. The data were expressed as the growth inhibition percentage calculated according to the equation: % growth inhibition = $100 - [(A_D \times 100)/A_B]$, where A_D is the measured absorbance in wells containing samples and A_B is the absorbance measured for blank wells (cells with a medium and a vehicle). To calculate the growth inhibitory potency of the compounds, concentration−response curves of the compounds were constructed and fitted to the following equation:

$$y = E_{max} / [1 + (IC_{50} / x)^n] \quad (7)$$

where y is the percentage growth inhibitory effect, E_{max} is the maximal inhibitory effect observed, IC_{50} is the concentration of the compound inhibiting the growth to 50%, n is the slope of the fitting, x is the drug concentration, and n is the slope. Nonlinear regression was carried out by *GraphPad Prism*, version 2.01, 1996 (GraphPad Software Inc.).

Inhibition of CDK1. The activity of CDK1 was quantified by a mobility shift assay. Simplified method: the CDK1 kinase (0.5 nM, Carna Biosciences 04-102) was added to a 384-well plate (Greiner 781076). The selected compounds and substrate FL-Peptide 29 (1.5 μM, ProfilerPro-Caliper 760429) + ATP (55 μM, Sigma A2383) were added. The mixture was incubated for 1 h without stirring. Then, the termination buffer (40 μL, ProfilerPro-Caliper 760367) + EDTA (40 mM, Sigma ED2SS) were added. Formation of the product was detected by LabChip EZ Reader II (PerkinElmer). The inhibition percentage was calculated with respect to inhibitor absence points (0% inhibition) and ATP absence points (100% inhibition).

X-ray Crystallography. A summary of the crystal data collection and refinement parameters for all compounds is given in Table 2SI-a,b in the SI. Single crystals of [**1a**]**Cl**·2H_2O, [**1b**](BF_4)·2H_2O, [**1c**](BF_4)·H_2O, [**2c**]**Cl**, {[**4b**](BF_4)(SiF_6)$_{0.5}$}·2H_2O, [**5c**](PF_6)$_2$·H_2O, and [**7c**] were mounted on a glass fiber and transferred to a Bruker X8 APEX II CCD-based diffractometer equipped with a graphite-monochromated Mo Kα radiation source (λ = 0.71073 Å). The highly redundant data sets were integrated using *SAINT*[51] and corrected for Lorentz and polarization effects. The absorption correction was based on the function fitting to the empirical transmission surface as sampled by multiple equivalent measurements with the program *SADABS*.[52]

The software package *SHELXTL*, version 6.10,[53] was used for space group determination, structure solution, and refinement by full-matrix least-squares methods based on F^2. A successful solution by direct methods provided most non-H atoms from the *E* map. The remaining non-H atoms were located in an alternating series of least-squares cycles and difference Fourier maps. All non-H atoms were refined with anisotropic displacement coefficients. H atoms were placed using a "riding model" and included in the refinement at calculated positions. CCDC reference numbers for [**1a**]**Cl**·2H_2O, [**1b**](BF_4)·2H_2O, [**1c**](BF_4)·H_2O, [**2c**]**Cl**, {[**4b**](BF_4)(SiF_6)$_{0.5}$}·2H_2O, [**5c**](PF_6)$_2$·H_2O, and [**7c**] are 996487−996493, respectively.

■ ASSOCIATED CONTENT

Ⓢ Supporting Information

X-ray crystallographic data in CIF format, ^{1}H and ^{19}F NMR and 2D ^{1}H−^{1}H NOESY spectra, crystal data and structure refinement, selected geometric parameters, $\pi-\pi$ stacking interaction, hydrogen bonds, representation showing centrosymmetric dimers, absorbance spectra, acid−base equilibria, and absorbance kinetic curves. This material is available free of charge via the Internet at http://pubs.acs.org.

■ AUTHOR INFORMATION

Corresponding Authors

*E-mail: begar@ubu.es.

*E-mail: gespino@ubu.es.

Notes

The authors declare no competing financial interest.

■ ACKNOWLEDGMENTS

Financial support by Obra Social "la Caixa" (Project OSLC-2012-007), Junta de Castilla y León (Fondo Social Europeo, Project BU-299A12-1), and MICINN Projects CTQ2011-24434 and CTQ2009-13051/BQU partially supported by FEDER, Spain, is gratefully acknowledged. We are also indebted to J. Delgado, P. Castroviejo, and M. Mansilla, from PCI of the University of Burgos, for technical support.

■ REFERENCES

(1) *Global Cancer—Facts & Figures*; American Cancer Society: Atlanta, GA, 2013; p. 1.

(2) Nicolaou, K. C.; Montagnon, T. *Molecules that changed the world: A brief history of the art and science of synthesis and its impact on society*; Wiley-VCH: Weinheim, Germany, 2008; p 208.

(3) Romero-Canelon, I.; Sadler, P. J. *Inorg. Chem.* **2013**, *52*, 12276−12291.

(4) (a) Süss-Fink, G. *Dalton Trans.* **2010**, *39*, 1673−1688. (b) Bratsos, L.; Jedner, S.; Gianferrara, T.; Alessio, E. *Chimia* **2007**, *61*, 692−697. (c) Sava, G.; Bergamo, A.; Dyson, P. J. *Dalton Trans.* **2011**, *40*, 9069−9075.

(5) (a) Fricker, S. P. *Dalton Trans.* **2007**, 4903−4917. (b) Wheate, N. J.; Walker, S.; Craig, G. E.; Oun, R. *Dalton Trans.* **2010**, *39*, 8113−8127.

(6) (a) Stepanenko, I. N.; Casini, A.; Edafe, F.; Novak, M. S.; Arion, V. B.; Dyson, P. J.; Jakupec, M. A.; Keppler, B. K. *Inorg. Chem.* **2011**, *50*, 12669−12679. (b) Stepanenko, I. N.; Novak, M. S.; Muhlgassner, G.; Roller, A.; Hejl, M.; Arion, V. B.; Jakupec, M. A.; Keppler, B. K. *Inorg. Chem.* **2011**, *50*, 11715−11728. (c) Ginzinger, W.; Muhlgassner, G.; Arion, V. B.; Jakupec, M. A.; Roller, A.; Galanski, M.; Reithofer, M.; Berger, W.; Keppler, B. K. *J. Med. Chem.* **2012**, *55*, 3398−3413. (d) Yellol, G. S.; Donaire, A.; Yellol, J. G.; Vasylyeva, V.; Janiak, C.; Ruiz, J. *Chem. Commun.* **2013**, *49* (98), 11533−11535.

(7) (a) Busto, N.; Valladolid, J.; Aliende, C.; Jalón, F. A.; Manzano, B. R.; Rodríguez, A. M.; Gaspar, J. F.; Martins, C.; Biver, T.; Espino, G.; Leal, J. M.; García, B. *Chem.—Asian J.* **2012**, *12*, 788−801. (b) Busto, N.; Valladolid, J.; Martínez-Alonso, M.; Lozano, H. J.; Jalón, F. A.;

Manzano, B. R.; Rodríguez, A. M.; Carrión, M. C.; Biver, T.; Leal, J. M.; Espino, G.; García, B. *Inorg. Chem.* **2013**, *52*, 9962−9974.
(8) Valladolid, J.; Hortigüela, C.; Busto, N.; Espino, G.; Rodríguez, A. M.; Leal, J. M.; Jalón, F. A.; Manzano, B. R.; Carbayo, A.; García, B. *Dalton Trans.* **2014**, *43*, 2629−2645.
(9) Aliende, C.; Pérez-Manrique, M.; Jalón, F. A.; Manzano, B. R.; Rodríguez, A. M.; Cuevas, J. V.; Espino, G.; Martínez, M. Á.; Massaguer, A.; González-Bártulos, M.; de Llorens, R.; Moreno, V. *J. Inorg. Biochem.* **2012**, *117*, 171−188.
(10) Bansal, Y.; Silakari, O. *Bioorg. Med. Chem.* **2012**, *20*, 6208−6236.
(11) Narasimhan, B.; Sharma, D.; Kumar, P. *Med. Chem. Res.* **2012**, *21*, 269−283.
(12) (a) Casas, J. S.; Castineiras, A.; García-Martínez, E.; Parajo, Y.; Perez-Paralle, M. L.; Sánchez-González, A.; Sordo, J. *Z. Anorg. Allg. Chem.* **2005**, *631*, 2258−2264. (b) Mock, C.; Puscasu, I.; Rauterkus, M. J.; Tallen, G.; Wolff, J. E. A.; Krebs, B. *Inorg. Chim. Acta* **2001**, *319*, 109−116.
(13) Ong, J. X.; Yap, C. W.; Ang, W. H. *Inorg. Chem.* **2012**, *51*, 12483−12492.
(14) Liu, H.-K.; Sadler, P. J. *Acc. Chem. Res.* **2011**, *44*, 349−359.
(15) Bugarcic, T.; Novakova, O.; Halamikova, A.; Zerzankova, L.; Vrana, O.; Kasparkova, J.; Habtemariam, A.; Parsons, S.; Sadler, P. J.; Brabec, V. *J. Med. Chem.* **2008**, *51*, 5310−5319.
(16) Blanck, S.; Maksimoska, J.; Baumeister, J.; Harms, K.; Marmorstein, R.; Meggers, E. *Angew. Chem., Int. Ed.* **2012**, *51*, 5244−5246.
(17) Lin, Y.; Huang, Y.; Zheng, W.; Wang, F.; Habtemariam, A.; Luo, Q.; Li, X.; Wu, K.; Sadler, P. J.; Xiong, S. *J. Inorg. Biochem.* **2013**, *128*, 77−84.
(18) Zeng, F. L.; Yu, Z. K. *Organometallics* **2008**, *27*, 2898−2901.
(19) (a) Davies, D. L.; Al-Duaij, O.; Fawcett, J.; Giardiello, M.; Hilton, S. T.; Russell, D. R. *Dalton Trans.* **2003**, 4132−4138. (b) Boutadla, Y.; Davies, D. L.; Jones, R. C.; Singh, K. *Chem.—Eur. J.* **2011**, *17*, 3438−3448.
(20) Ganter, C. *Chem. Soc. Rev.* **2003**, *32*, 130−138.
(21) (a) Kandioller, W.; Hartinger, C. G.; Nazarov, A. A.; Bartel, C.; Skocic, M.; Jakupec, M. A.; Arion, V. B.; Keppler, B. K. *Chem.—Eur. J.* **2009**, *15*, 12283−12291. (b) Mendoza-Ferri, M. G.; Hartinger, C. G.; Nazarov, A. A.; Eichinger, R. E.; Jakupec, M. A.; Severin, K.; Keppler, B. K. *Organometallics* **2009**, *28*, 6260−6265.
(22) Pettinari, R.; Pettinari, C.; Marchetti, F.; Cavel, C. M.; Scopelliti, R.; Dyson, P. J. *Organometallics* **2013**, *32*, 309−316.
(23) (a) Canivet, J.; Karmazin-Brelot, L.; Süss-Fink, G. *J. Organomet. Chem.* **2005**, *690*, 3202−3211. (b) Dykeman, R. R.; Luska, K. L.; Thibault, M. E.; Jones, M. D.; Schlaf, M.; Khanfar, M.; Taylor, N. J.; Britten, J. F.; Harrington, L. *J. Mol. Catal. A: Chem.* **2007**, *277*, 233−251.
(24) Pachhunga, K.; Therrien, B.; Kreisel, K. A.; Yap, G. P. A.; Kollipara, M. R. *Polyhedron* **2007**, *26*, 3638−3644.
(25) Bugarcic, T.; Habtemariam, A.; Stepankova, J.; Heringova, P.; Kasparkova, J.; Deeth, R. J.; Johnstone, R. D. L.; Prescimone, A.; Parkin, A.; Parsons, S.; Brabec, V.; Sadler, P. J. *Inorg. Chem.* **2008**, *47*, 11470−11486.
(26) (a) Chen, H. M.; Parkinson, J. A.; Parsons, S.; Coxall, R. A.; Gould, R. O.; Sadler, P. J. *J. Am. Chem. Soc.* **2002**, *124*, 3064−3082. (b) Chen, H. M.; Parkinson, J. A.; Novakova, O.; Bella, J.; Wang, F. Y.; Dawson, A.; Gould, R.; Parsons, S.; Brabec, V.; Sadler, P. J. *Proc. Natl. Acad. Sci. U. S. A.* **2003**, *100*, 14623−14628.
(27) Perez, J.; Riera, L. *Chem. Commun.* **2008**, 533−543.
(28) Schuecker, R.; John, R. O.; Jakupec, M. A.; Arion, V. B.; Keppler, B. K. *Organometallics* **2008**, *27*, 6587−6595.
(29) Fox, M. A.; MacBride, J. A. H.; Wade, K. *Polyhedron* **1997**, *16*, 2499−2507.
(30) (a) Gelmboldt, V. O.; Ganin, E. V.; Fonari, M. S.; Simonov, Y. A.; Koroeva, L. V.; Ennan, A. A.; Basok, S. S.; Shova, S.; Kahlig, H.; Arion, V. B.; Keppler, B. K. *Dalton Trans.* **2007**, 2915−2924. (b) Fernández-Galán, R.; Manzano, B. R.; Otero, A.; Lanfranchi, M.; Pellinghelli, M. A. *Inorg. Chem.* **1994**, *33*, 2309−2312.
(31) (a) Demoro, B.; de Almeida, R. F. M.; Marques, F.; Matos, C. P.; Otero, L.; Pessoa, J. C.; Santos, I.; Rodríguez, A.; Moreno, V.; Lorenzo, J.; Gambino, D.; Tomaz, A. I. *Dalton Trans.* **2013**, *42*, 7131−7146. (b) Almodares, Z.; Lucas, S. J.; Crossley, B. D.; Basri, A. M.; Pask, C. M.; Hebden, A. J.; Phillips, R. M.; McGowan, P. C. *Inorg. Chem.* **2014**, *53*, 727−736. (c) Lucas, S. J.; Lord, R. M.; Wilson, R. L.; Phillips, R. M.; Sridharan, V.; McGowan, P. C. *Dalton Trans.* **2012**, *41* (45), 13800−13802.
(32) (a) Kilpin, K. J.; Clavel, C. M.; Edafe, F.; Dyson, P. J. *Organometallics* **2012**, *31*, 7031−7039. (b) Mendoza-Ferri, M. G.; Hartinger, C. G.; Nazarov, A. A.; Eichinger, R. E.; Jakupec, M. A.; Severin, K.; Keppler, B. K. *Organometallics* **2009**, *28*, 6260−6265. (c) Stepanenko, I. N.; Casini, A.; Edafe, F.; Novak, M. S.; Arion, V. B.; Dyson, P. J.; Jakupec, M. A.; Keppler, B. K. *Inorg. Chem.* **2011**, *50*, 12669−12679.
(33) (a) Loughrey, B. T.; Healy, P. C.; Parsons, P. G.; Williams, M. L. *Inorg. Chem.* **2008**, *47*, 8589−8591. (b) Walker, J. M.; McEwan, A.; Pycko, R.; Tassotto, M. L.; Gottardo, C.; Th'ng, J.; Wang, R. Y.; Spivak, G. J. *Eur. J. Inorg. Chem.* **2009**, 4629−4633. (c) Romero-Canelon, I.; Salassa, L.; Sadler, P. J. *J. Med. Chem.* **2013**, *56*, 1291−1300. (d) Mitra, R.; Das, S.; Shinde, S. V.; Sinha, S.; Somasundaram, K.; Samuelson, A. G. *Chem.—Eur. J.* **2012**, *18*, 12278−12291.
(34) Habtemariam, A.; Melchart, M.; Fernández, R.; Parsons, S.; Oswald, I. D. H.; Parkin, A.; Fabbiani, F. P. A.; Davidson, J. E.; Dawson, A.; Aird, R. E.; Jodrell, D. I.; Sadler, P. J. *J. Med. Chem.* **2006**, *49*, 6858−6868.
(35) Wang, F.; Habtemariam, A.; van der Geer, E. P. L.; Fernández, R.; Melchart, M.; Deeth, R. J.; Aird, R.; Guichard, S.; Fabbiani, F. P. A.; Lozano-Casal, P.; Oswald, I. D. H.; Jodrell, D. I.; Parsons, S.; Sadler, P. J. *Proc. Natl. Acad. Sci. U. S. A.* **2005**, *102*, 18269−18274.
(36) Peacock, A. F. A.; Sadler, P. J. *Chem.—Asian J.* **2008**, *3*, 1890−1899.
(37) (a) Chen, H.; Parkinson, J. A.; Morris, R. E.; Sadler, P. J. *J. Am. Chem. Soc.* **2002**, *125*, 173−186. (b) Novakova, O.; Chen, H.; Vrana, O.; Rodger, A.; Sadler, P. J.; Brabec, V. *Biochemistry* **2003**, *42*, 11544−11554.
(38) Ronconi, L.; Sadler, P. J. *Coord. Chem. Rev.* **2007**, *251*, 1633−1648.
(39) Haga, M.-A. *Inorg. Chim. Acta* **1983**, *75*, 29−35.
(40) Chang, Y.-M.; Chen, C. K. M.; Hou, M.-H. *Int. J. Mol. Sci.* **2012**, *13*, 3394−3413.
(41) García, B.; Leal, J. M.; Ruiz, R.; Biver, T.; Secco, F.; Venturini, M. *J. Phys. Chem. B* **2010**, *114*, 8555−8564.
(42) Kostrhunova, H.; Vrana, O.; Suchankova, T.; Gibson, D.; Kasparkova, J.; Brabec, V. *Chem. Res. Toxicol.* **2010**, *23*, 1833−1842.
(43) He, L.; Liao, S. Y.; Tan, C. P.; Ye, R. R.; Xu, Y. W.; Zhao, M.; Ji, L. N.; Mao, Z. W. *Chem.—Eur. J.* **2013**, *19*, 12152−12160.
(44) Loughrey, B. T.; Healy, P. C.; Parsons, P. G.; Williams, M. L. *Inorg. Chem.* **2008**, *47*, 8589−8591.
(45) Bennett, M. A.; Smith, A. K. *J. Chem. Soc., Dalton Trans.* **1974**, 233−241.
(46) Soleimannejad, J.; White, C. *Organometallics* **2005**, *24*, 2538−2541.
(47) Zeng, F. L.; Yu, Z. K. *Organometallics* **2008**, *27*, 2898−2901.
(48) (a) Chiswell, B.; Lions, F.; Morris, B. S. *Inorg. Chem.* **1964**, *3*, 110−113. (b) Stupka, G.; Gremaud, L.; Williams, A. F. *Helv. Chim. Acta* **2005**, *88*, 487−495.
(49) Fulmer, G. R.; Miller, A. J. M.; Sherden, N. H.; Gottlieb, H. E.; Nudelman, A.; Stoltz, B. M.; Bercaw, J. E.; Goldberg, K. I. *Organometallics* **2011**, *29*, 2176−2179.
(50) Carmichael, J.; DeGraff, W. G.; Gazdar, A. F.; Minna, J. D.; Mitchell, J. B. *Cancer Res.* **1987**, *47*, 943−946.
(51) *SAINT+, Area-Detector Integration Program*, version 7.12a; Bruker AXS Inc.: Madison, WI, 2004.
(52) Sheldrick, G. M. *SADABS, A Program for Empirical Absorption Correction*, version 2004/1; University of Göttingen: Göttingen, Germany, 2004.
(53) *SHELXTL-NT Structure Determination Package*, version 6.12; Bruker AXS Inc.: Madison, WI, 2001.

dx.doi.org/10.1021/ic501865h | *Inorg. Chem.* XXXX, XXX, XXX−XXX